BIOCHEMISTRY
including biophysical chemistry & molecular biology

# Structural and Functional Assessment of Perilipin 2 Lipid Binding Domain(s)

Charles P. Najt,[#,‡] Joel S. Lwande,[#,‡] Avery L. McIntosh,[§] Subramanian Senthivinayagam,[‡] Shipra Gupta,[‡] Leslie A. Kuhn,[‡,†] and Barbara P. Atshaves*[,‡]

[‡]Department of Biochemistry and Molecular Biology and [†]Department of Computer Science and Engineering, Michigan State University, East Lansing, Michigan 48824, United States

[§]Physiology and Pharmacology, Texas A&M University, TVMC College Station, Texas 77843-4466, United States

Ⓢ Supporting Information

ABSTRACT: Although perilipin 2 (Plin2) has been shown to bind lipids with high affinity, the Plin2 lipid binding site has yet to be defined. This is of interest since Plin2's affinity for lipids has been suggested to be important for lipid droplet biogenesis and intracellular triacylglycerol accumulation. To define these regions, mouse Plin2 and several deletion mutants expressed as recombinant proteins and in mammalian cells were assessed by molecular modeling, fluorescence binding, circular dichroic, and fluorescence resonance energy transfer techniques to identify the structural and functional requirements for lipid binding. Major findings of this study indicate (1) the N-terminal PAT domain does not bind cholesterol or stearic acid; (2) Plin2 residues 119−251, containing helix α4, the α−β domain, and part of helix α6 form a Plin3-like cleft found to be important for highest affinity lipid binding; (3) both stearic acid and cholesterol interact favorably with the Plin2 cleft formed by conserved residues in helix α6 and adjacent strands, which is common to all the active lipid-binding constructs; and (4) discrete targeting of the Plin2 mutants to lipid droplets supports Plin2 containing two independent, nonoverlapping lipid droplet targeting domains in its central and C-terminal sequences. Thus, the current work reveals specific domains responsible for Plin2−lipid interactions that involves the protein's lipid binding and targeting functions.
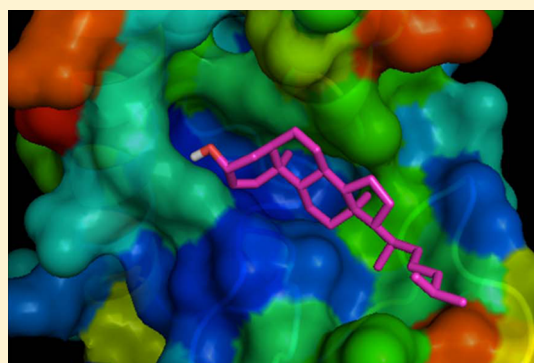
The lipid droplet protein perilipin 2 (Plin2, also known as adipose differentiation-related protein, ADRP, or adipophilin) has been shown to play a key role in lipid droplet formation[1] and intracellular triglyceride accumulation[1−4] and to bind lipids with high affinity,[5−8] yet little is known about the structure or location of its lipid binding site(s). This represents a significant gap in knowledge since there is evidence that Plin2's binding capacity may influence several lipid parameters including fatty acid uptake,[9] high density lipoprotein (HDL)-mediated cholesterol uptake/efflux,[8,10] and very low density lipoprotein (VLDL) content in mouse models of obesity.[11] In fact, a genetic variation in the *Plin2* gene causing a serine to proline mutation (Ser251Pro) results in dysregulation of plasma lipid and lipoprotein profiles in humans,[12] possibly due to disruption of helical structure within a putative lipid binding site. As part of the Plin (or PAT, for *p*erilipin/*A*DRP/*T*IP47) family of lipid droplet targeting proteins which includes Plin1/perilipin, Plin2/ADRP, Plin3/TIP47, Plin4/S3−12, and Plin5/OXPAT, Plin2 shares high sequence homology with members of the group.[13] With Plin1[14] and other lipid droplet-associated proteins such as caveolins,[15] the targeting and anchoring of proteins depends on targeting signals in the form of hydrophobic sequences. These signals are not, however, conserved in Plin2,[14] suggesting different lipid droplet targeting mechanisms exist among lipid droplet associated proteins. In support of this, Plin2 contains two lipid droplet targeting domains that are not hydrophobic in nature.[16,17] These domains are nonoverlapping suggesting that targeting of Plin2 to lipid droplets is controlled by the tertiary structure in which contributing residues are brought together to form the targeting signal.[16,17] Likewise, the lipid binding site of Plin2 may also be defined by the tertiary structure of the protein and may not be easily described by a linear sequence motif. In keeping with this, there is evidence that binding of cholesterol and other lipids by membrane proteins often occurs in grooves between helices and involves conserved spatial motifs.[18−21] On the basis of sequence similarity[22] and predicted structure,[16,17] several conserved regions within Plin2 have the potential to bind lipids including (1) a highly conserved N-terminal hydrophobic domain (residues 1−115) known as the PAT domain[22,23] that is involved in lipid droplet stabilization, lipid accumulation, and proteasomal degradation of Plin2;[23,24] (2) the N-terminal 11-mer repeating domain located within residues 103−215[25,26] that is believed to participate with part

of the C-terminal domain to regulate secretion of milk lipids by forming an adaptive link between lipid droplets and the plasma membrane;[27] (3) two predicted lipid droplet targeting domains in the middle and C-terminal regions of the protein;[16,17] and (4) a C-terminal $\alpha-\beta$ domain and a 4-helix bundle domain reminiscent of the LDL receptor binding domain of apolipoprotein E.[25] The last structure was predicted based on homology between Plin2 and the known crystal structure of the closely related Plin3.[25] In Plin3, the $\alpha-\beta$ domain and 4-helix bundle fold together into an L-shape, forming a cleft (13 Å at its widest, 18 Å long, and 10 Å deep) with several hydrophobic residues and a deep polar pocket of sufficient size to accommodate lipid ligands and interact with their polar groups. Since Plin2 and Plin3 share 42% overall sequence identity throughout and 35% identity in the C-terminal region (NCBI BLAST), substantial structural similarity is expected. In fact, a comprehensive study has shown that sequences with at least 25% identity over at least 80 residues have backbone structures that overlay closely.[28] Recently, a structural model was presented for Plin2 based on sequence similarity to the known three-dimensional structures of Plin3, apolipoprotein A1, the signal receiver domain of a putative luxo repressor protein, and dihydroorotate reductase.[29] Work presented here supports that an apolipophorin-like N-terminal domain and a Plin3-like C-terminal domain together can account for the overall tertiary fold of Plin2. Others have noted structural similarities between apolipoproteins and the N-terminal domain of Plin proteins.[25] Both contain 11-mer repeats (located within helix $\alpha4$ and the $\alpha-\beta$ domain in Plin2) that are found in other lipid- or membrane-associated proteins including phosphate cytidyltransferases and synucleins,[30] suggesting these domains may serve as lipid interacting sites in these proteins. In support of these findings, others have shown that structure predictions of 11-mer repeats, such as those described in the N-terminal regions of Plin2 and Plin3, do not produce stable helical entities in proteins such as synucleins[29,30] and only adopt a helical structure upon interaction of lipid ligands or lipid membranes.[31] Interestingly Bulankina et al. demonstrated that the 11-mer repeat region in Plin3 interacted with lipid droplet membranes through residues 87−198.[32] Moreover, it was suggested that Plin3 adopts a distinct N-terminal and C-terminal structure that extends upon membrane interaction to accommodate the lipid structure and cause lipid reorganization.[32] Thus, despite structural similarities between Plin2 and Plin3, differences in the N-terminal and C-terminal regions contribute to the distinct functions of the proteins.

The present investigation was undertaken to examine the structure and location of the Plin2 lipid binding site(s) within conserved domains by characterizing Plin2 and several deletion mutants using molecular modeling, fluorescence binding, circular dichroism, and fluorescence resonance energy transfer (FRET) techniques. Evidence is provided that lipid binding by Plin2 does not require the full-length protein but instead employs residues from two helical bundle domains for highest affinity lipid binding and targeting to lipid droplets, activities that are dependent on strong Plin2-lipid or Plin2-membrane interactions. Crucial residues within these domains are 119−251, a region that contains helix $\alpha4$, the $\alpha-\beta$ domain ($\alpha5$, $\beta3$), and part of helix $\alpha6$, included in the cleft region. Residues within ConSurf analysis shows that surface-exposed residues within the cleft are highly conserved and likely to be functionally important. Furthermore, flexible docking of stearic

acid and cholesterol into this region indicates favorable interactions with both ligands and the cleft formed from a polar pocket with surrounding hydrophobic residues. Since mutations in this region of Plin2 resulted in dysregulation of plasma lipid and lipoprotein profiles in humans,[12] study of the functional importance of this area is warranted.

■ MATERIALS AND METHODS

Materials. Cholesterol and stearic acid were purchased from Sigma (St. Louis, MO). NBD-cholesterol and NBD-stearic acid were obtained from Molecular Probes (Eugene, OR). Expression vector pQE9-His was purchased from Addgene (Cambridge, MA). CFP-fusion protein expression vector pECFP-N1 was purchased from BD Biosciences (BD Biosciences Clontech, Palo Alto, CA). Ni-NTA resin and M15 cells for protein expression were obtained from Qiagen (Chatsworth, CA). Rabbit anti-Plin2 polyclonal antibody was prepared as described.[33] Lipofectamine 2000 was purchased from Life Technologies-Invitrogen (Carlsbad, CA).

Buffers. Buffer A contained 50 mM Na_2HPO_4 (pH 8.0), 300 mM NaCl, and protease inhibitors (1 tablet per 50 mL). Buffer B contained 20 mM Tris-HCl (pH 7.9), 100 mM Na_2HPO_4, 500 mM NaCl and 20 mM imidazole and 6 M guanidine hydrochloride. Buffer C contained 20 mM Tris-HCl (pH 7.9), 500 mM NaCl, 20 mM imidazole, and 6 M urea. Buffer D was Buffer C at pH = 5.9. Buffer E was 10 mM Tris-HCl (pH 7.5), and 150 mM NaCl. Buffer F contained PBS, 2 mM EDTA, 10 mM DTT, and protease inhibitors. Buffer G contained PBS, 10 mM DTT, 0.1% SDS and 10% glycerol. Buffer H was PBS, 10 mM DTT, and 2 M urea. Buffer I was Buffer H in 8 M urea. Buffer J was Buffer E at pH 8.3 plus 20 mM imidazole. Buffer K was Buffer J at pH 7.5. Buffer L was Buffer E plus 50 mM EDTA.

Plasmids. The full coding sequence of mouse Plin2 cDNA was cloned into pQE9-His vector (Origene, Rockville, MD) following standard procedures. Unique restriction sites *Bam*HI and *Hin*dIII were introduced by PCR amplification with the following forward and reverse primers: Plin2-forward, 5′-CAC GGA TCC ATG GCA GCA GCA GTA GTA GAT CCG CAA C-3′ and Plin2-reverse, 5′-GTG AAG CTT TTA CTG AGC TTT GAC CTC-3′. The forward primer was designed with a silent mutation where guanine was replaced by adenine in the Plin2 sequence to remove a *Bam*HI site located within the first 18 bp of the Plin2 gene. By cloning Plin2 cDNA into the pQE9-His vector, an N-terminal His-Tagged fusion protein was formed upon expression that allowed recombinant protein to be purified using Ni-NTA based affinity chromatography. Expression plasmids for the deletion mutants were generated from the above construct by site-directed mutagenesis as described elsewhere[34] using the following primers: Plin2-C1 forward, 5′-CAT CAC GGA TCC ATG ACG ACT ACC ATG GCT GGA GCC-3′; Plin2-C1 reverse, 5′-AGC CAT GGT AGT CGT CAT GGA TCC GTG ATG GTG ATG-3′; Plin2-C2 forward, 5′-CAT CAC GGA TCC ATG GTC CAC CTG ATT GAA TTC GCC-3′; Plin2-C2 reverse, 5′-TTC AAT CAG GTG GAC CAT GGA TCC GTG ATG GTG ATG-3′; Plin2-N1 forward, 5′-GAT GTG ACG ACT TAA AAG CTT AAT TAG CTG AGC-3′; Plin2-N1 reverse, 5′-CTA ATT AAG CTT TTA AGT CGT CAC ATC CTT CGC-3′; Plin2-N2 forward, 5′-ACC ATT TCT CAG CTC TAA AAG CTT AAT TAG CTG AGC-3′; Plin2-N2 reverse, 5′-CTA ATT AAG CTT TTA GAG CTG AGA AAT GGT CTC CTG-3′. Plin2-I was made using Plin2-C1 as the template DNA and the primers

used for creating Plin2-N2. The resulting plasmids were sequenced to ensure fidelity and identity.

Expression and Purification of Recombinant Proteins in *Escherichia coli* Cells. Recombinant Plin2 and the deletion mutants were purified as previously described with some modifications.[5] Briefly, proteins were overexpressed in *E. coli* host strain M15 and grown at 37 °C in 1 L cultures containing 2X-YT medium with 100 μg/mL ampicillin until OD_{600} = 0.8, followed by induction with IPTG (1 mM). After 1 h, cells were harvested by centrifugation (4 °C for 30 min at 3500g). For purification of Plin2, Plin2-I, Plin2-N1, and Plin2-N2, pelleted cells were resuspended in Buffer A then sonicated. Lysates were centrifuged at 4 °C for 15 min at 25000g, and the pellet was solubilized in Buffer B and applied to a Ni-NTA column equilibrated in Buffer B. The column was sequentially washed with buffers B, C and D, and E. The protein was eluted using Buffer L and then checked for purity by SDS-PAGE analysis. For deletion mutants Plin2-C1 and Plin2-C2, the pelleted cells were resuspended in Buffer F, sonicated, and centrifuged at 4 °C for 15 min at 25000g. The resulting pellet was washed 2× each with buffers G and H, solubilized in Buffer I, and centrifuged at 4 °C for 15 min at 25000g. The supernatant was then sequentially dialyzed against PBS containing 10 mM DTT in decreasing concentrations of urea (6, 5, and 4 M urea). The protein in 4 M urea was then loaded onto a Ni-NTA column equilibrated in Buffer J. The column was then sequentially washed with the buffers J and K, and then eluted with Buffer L. Analysis by SDS-PAGE and Western blotting as described in ref 4 allowed assignment of protein purity.

Plin2 Structural Prediction and Analysis. The Hopp and Woods hydropathy analysis method[35] (web server: http://www.vivo.colostate.edu/molkit/hydropathy/index.html) was used to predict hydrophilic and hydrophobic segments within Plin2 based on a hydrophilicity index assigned to the amino acids, averaged over six successive residues. The PAT domain and two lipid droplet targeting domains in Plin2 were previously described.[17,24,26] The secondary structure of Plin2 was predicted by the PredictProtein server at http://www.predictprotein.org.[36] This method has greater than 72% accuracy, on average, in assigning α-helical, β-strand (extended) or loop conformation to protein residues. Secondary structural predictions of the Plin2 N-terminal region (residues 1−171) were consistent with further analysis by PSIPRED,[37,38] SAM,[39] and SABLE2.[40] On the basis of their significant (35%) sequence identity, the Plin2 C-terminal domain structure was modeled by homology to the structure of residues 209−431 in Plin3[25] from Protein Data Bank entry 1SZI[41] by using Modeler,[42,43] as implemented in the ModWeb Web server (salilab.org/modweb). Given the absence of close homologues of known structure to the Plin2 N-terminal region, this sequence was submitted for analysis by the Pcons fold recognition web server (http://pcons.net/) to identify the three-dimensional structural fold providing the most compatible amino acid environments and secondary structures. By comparing the top-scoring predictions from 11 different three-dimensional modeling methods (Pcons, Pmodeller, PconsM, blast, forte, fugue, hhpred2, nfold, rpsblast, sam-t02, and sam-t08), Pcons selected the structural model for the N-terminal Plin2 region showing the highest degree of structural consensus among the results. The degree of amino acid conservation within 38 homologues of the C-terminal domain of ADRP was assessed by ConSurf (http://consurf.tau.ac.il/), which automatically detects homologues, performs multiple sequence

alignment, and maps amino acid conservation values onto the structure.[44,45] Molecular graphics figures were rendered using PYMOL (Schrödinger, LLC).[33] Stearic acid interactions with the modeled Plin2 C-terminal domain were assessed by extracting the 3-dimensional structure of stearic acid from the PDB X-ray structure 1HMT.[46] Partial charges were assigned to its atoms with Molcharge v. 1.3.1 software from OpenEye Scientific Software (http://www.eyesopen.com; Santa Fe, NM). Low-energy (favorable) flexible conformations of highly flexible stearic acid were then generated by using Omega2 v. 2.3.2 (also from OpenEye Scientific Software). Similarly, the 3-dimensional structure of cholesterol (residue 3001D) was extracted from PDB entry 3KDP.[47] Partial charges were assigned with Molcharge, and low-energy conformations of the cholesterol hydrophobic tail were sampled with Omega2. The stearic acid and cholesterol conformers were evaluated for their ability to interact favorably with the conserved cleft in the 3-dimensional model of the C-terminal domain structure of Plin2 by using SLIDE version 3.3.5 software to dock each conformer of stearic acid or cholesterol into the cleft between the $\alpha−\beta$ domain and 4-helix bundle, and selecting the orientation and conformation with the most favorable predicted $\Delta G_{binding}$ to Plin2, as assessed by SLIDE AffiScore. SLIDE models side-chain flexibility in both molecules during docking.[48]

Cells Culture and Transfections. Mouse L cell fibroblasts expressing CFP-labeled Plin2 and the deletion mutants were generated as described[4] using mammalian expression vector pECFP-N1 and unique restriction sites (*Xho*I, *Kpn*I) introduced by PCR. Resulting expression plasmids were sequenced to verify identity and fidelity and then stably transfected into L cells using Lipofectamine 2000 from Life Technologies (Grand Island, NY) according to the manufacturer's instructions. Clones surviving selection with G418 were cell-sorted for strong CFP signal under sterile conditions using an INFLUX cell sorter (BD scientific, Palo Alto, CA) and screened by Western blot analysis and fluorescence imaging to ensure stable expression of CFP-labeled protein. Mock transfectants (clones transfected with vector DNA without insert) were generated in parallel and were designated as controls.

Urea Denaturation Studies. To show the effects of protein unfolding on Plin2 tryptophan residues, protein-denaturation studies in the presence of urea were performed as described.[49] In brief, the intrinsic tryptophan fluorescence (excitation 295 nm, emission 300−400 nm) of three Plin2 tryptophans located at positions 283, 286, and 398 was collected using a Cary Eclipse fluorescence spectrophotometer (Varian, Walnut Creek, CA) at constant temperature (25 °C) before and after addition of increasing amounts of urea (up 6 M) to Plin2 (100 nM) in 10 mM NaH_2PO_4, pH 7.5. Samples were allowed to equilibrate 2 min after addition of each urea aliquot. Data were corrected for background scatter originating from the buffer and analyzed to graphically show the tryptophan fluorescence spectrum at increasing urea concentrations and the percent fluorescence remaining after each addition.

Intrinsic Tryptophan Fluorescence Binding Studies. The binding of cholesterol and stearic acid to Plin2 was examined by measuring the fluorescence quenching of Plin2 tryptophan residues after addition of ligand as described.[50,51] In brief, the intrinsic tryptophan fluorescence of Plin2 (100 nM in 10 mM NaH_2PO_4, pH 7.5) was monitored from 300 to 400 nm

after excitation at 295 nm (to minimize interference from Plin2 tyrosine fluorescence) both before and after addition of increasing increments of cholesterol, stearic acid, arachidonic acid, and docosahexaenoic acid (up to 100 nM) using a Cary Eclipse fluorescence spectrophotometer. Data was corrected for background scatter originating from the buffer and increasing ligand without protein present. The intrinsic tryptophan fluorescence in the presence of different concentrations of ligand was plotted as the maximum fluorescence difference ($\Delta F = F_o - F$) vs ligand concentration to yield a saturation curve where F and F_o were the measured fluorescence emission intensity of the protein solution in the presence and absence of ligand, respectively. The dissociation constant K_d was determined from the double reciprocal plot of the saturation curve. Linear regression of $1/[1 - (F/F_{max})]$ versus [ligand]/(F/F_{max}) yielded a slope $= 1/K_d$ and ordinate intercept $= nE_o/K_d$ where F represented fluorescence intensity at a given concentration of ligand, Fmax was the maximal fluorescence, [ligand] was the ligand concentration, E_o was the protein concentration, and n equaled the number of ligand binding sites.

NBD-Labeled Ligand Binding Assays. Since not all of the deletion mutations contained tryptophan residues, a fluorescent ligand binding assay was developed using NBD-cholesterol and NBD-stearic acid as described.[5−8] In brief, NBD-labeled lipids were added incrementally (0−300 nM) to proteins (Plin2 and Plin2 deletion mutants) at 100 nM in phosphate buffer (10 mM, pH 7.5). Samples were allowed to mix 2−5 min after each addition before exciting at 469 nm. Fluorescence emission spectra were recorded from 490 to 600 nm and integrated. Data were corrected for both background scatter originating from the buffer and increasing ligand without protein present. A saturation curve developed by plotting fluorescence intensities vs ligand concentration and the double reciprocal plot of this curve allowed determination of K_d as discussed previously.

Colocalization Studies. To show the ability of Plin2 and the deletion mutants to target to lipid droplets, colocalization studies were performed as described[4,33] with cells expressing full-length Plin2 or one of the deletion constructs. Cells seeded at a density of 50 000 cells/well in 4-well chamber slides (EZ Slide, Millipore, Billerica, MA) were treated overnight with oleic acid (100 μM) 4−5 h after plating. After 16 h, cells were incubated with NBD-Cholesterol (2 μM) for 2 h, then fixed in 3.7% formaldehyde for 20 min at room temperature followed by washing (3×) with PBS. The cells were then blocked with 2% BSA and incubated with rabbit anti-CFP antibody (1:50) for 1 h at room temperature. Since the transfected cells express CFP-labeled proteins (as described above), anti-CFP was used in place of anti-Plin2 to discriminate endogenous Plin2 from the transfected mutant proteins. After extensive washing, cells were incubated with Cy5 labeled antirabbit secondary antibody (1:100) in 2% BSA for 1 h. Cells were washed with PBS and mounted with coverslips using fluorogel mounting medium (Electron Microscopy Science, Hatfield, PA). As a control, cells were also labeled with the Cy5-labeled secondary antibody alone. Images were acquired sequentially on an Olympus FluoView 1000 Laser Scanning Confocal Microscope (Olympus Inc., Center Valley, CA) equipped with an IX81 automated inverted microscope and operated with Fluoview software. Fluorescence emission was detected using 488 nm excitation and 500/100 band path emission filter for NBD-cholesterol (green channel) and 635 nm excitation with a 725/30 band

path filter for the Cy5 emission (red channel). To minimize photobleaching, samples were exposed to the light source for minimal time periods. Image files were analyzed using Metamorph software (West Chester, PA). Images derived from the red and green channels were combined and appeared as yellow to orange where superimposition of images derived from the red and green channels overlapped.

Fluorescence Resonance Energy Transfer Microscopy. Acceptor photobleaching experiments were performed as previously described[4,52] on cells labeled as described above by measuring the fluorescence emission of the NBD donor through the 500/100 nm filter upon excitation at 488 nm both before and after photobleaching of the Cy5-acceptor excited at 635 nm. Control experiments were performed to limit interference from nonspecific fluorescence including (1) imaging nonlabeled cells to determine autofluorescence in the green channel (NBD) while maintaining maximum dynamic range; (2) adjusting the gain and black levels in the red channel after excitation at 635 nm to limit fluorescence bleed-through into the green channel; (3) photobleaching NBD-labeled donor cells without Cy5 present to check for nonspecific fluorescent increases in the donor channel to ensure that the donor intensity was not affected by bleaching the cells; and (4) leaving one or two cells unbleached during the FRET experiment to serve as in-field bleaching control. To calculate the FRET efficiency (E), representing the efficiency of energy transfer between donor and acceptor, the following equation was used: $E = 1 - (I_{DA}/I_D)$ where I_{DA} is donor fluorescence intensity before acceptor photobleaching and I_D is the donor fluorescence intensity after acceptor photobleaching. An average E value was calculated from the NBD fluorescence emission increase after photobleaching. The intermolecular distance R between NBD-label and the Cy5-labeled Plin2 was calculated from the equation $R = R_0(1/E - 1)^{(1/6)}$, where E was experimentally determined and R_0 was the Förster radius for the NBD-Cy5 FRET pair (56 Å). Since accurate determination within the cellular environment of parameters of the probes (e.g., donor quantum yield, acceptor extinction coefficient, and dipole orientation factor between donor/acceptor pair) involved in the calculation of R_0 is difficult, interaction distances (R) were also presented in terms of R_0, with $R_0 < 75$ Å such that $\kappa^2 < 4$.[53]

Circular Dichroic Analysis of Secondary Structure. The far UV circular dichroic (CD) spectra of each protein was measured in phosphate buffer (10 mM NaH_2PO_4, pH 7.5 with 10 mM NaCl) in the presence and absence of ligand (cholesterol or stearic acid) to a final concentration of 5 μM. Experiments were performed at 25 °C in a 1 mm path length cuvette using a JASCO J-815 CD spectrometer (JASCO Analytical Instruments, Easton, MD). Experiments with ligand were allowed to incubate for 2−5 min prior to each scan to allow maximal protein−ligand interaction. CD spectra were recorded from 270 to 190 nm at a scan rate of 50 nm/min with a time constant of 1 s and bandwidth of 2 nm. For each experiment, 10 iterations were performed in triplicate. Secondary structure analysis was carried out using the CDSSTR analysis program[54] with results reported as percentages of regular α-helices, distorted α-helices, regular β-strands, distorted β-strands, turns and unordered structures. In a separate experiment, measurements on purified recombinant Plin2 were performed at 5 °C, 25 °C, and 40 °C to determine the dependence of secondary structure on temperature.
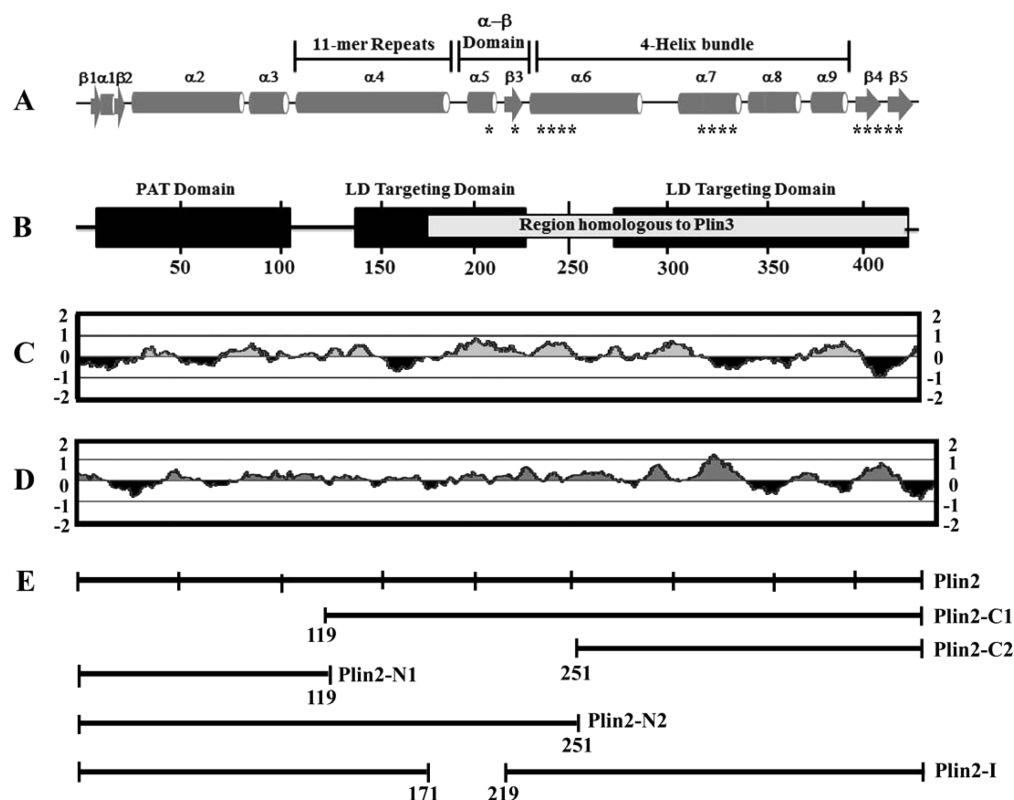
Figure 1. Predicted secondary structure and conserved domains of Plin2. On the basis of prediction software (SABLE2, SAM and PsiPRED) and the known X-ray crystal structure of the homologous Plin3 protein, the predicted structure of Plin2 (A) contains nine α-helices and five small β strands interconnected by random coils and unordered structure. Several regions of interest include the PAT domain (B), 11-mer repeat region (A), two lipid droplet (LD) targeting domains (B), and the C-terminal area containing an α−β domain (A) and 4-helix bundle (A) that together formed a cleft region. Residues that line the cleft (indicated by *) include Val-203, Tyr-215, Ala-233, Arg-236, Val-237, Ala-240, Thr-325, Val-326, Asn-329, Gln-331, Trp-398, Leu-399, Val-400, Pro-402 and Phe-403. Hopp-Woods hydrophilicity plots for Plin2 (C) and Plin3 (D) were generated using a server at the Colorado State University (http://www.vivo.colostate.edu/molkit/hydropathy/index.html) to provide predicted hydrophilic (lines above zero) and hydrophobic regions (below zero) within the proteins. Line diagrams of Plin2 and the deletion mutants (E) include full-length Plin2 (containing amino acid residues 1−425); Plin2-C1 (residues 119−425); Plin2-C2 (residues 251−425); Plin2-N1 (residues 1−119); and Plin2-N2 (residues 1−251); and Plin2-I (residues1−171 and 219−425).

Statistics. All values were expressed as the means ± SE. Statistical analyses were performed using Student's t test or one-way ANOVA with Newman Keuls posthoc test (GraphPad Prism, San Diego, CA) to determine statistical significance. Values with $P < 0.05$ or less were considered significant.

■ RESULTS

Prediction of Plin2 Secondary Structure and Conserved Domains. To understand how ligand binding relates to structure, the secondary structure of Plin2 was predicted using several prediction programs including PredictProtein,[36] PSIPRED,[37,38] SAM,[39] and SABLE2.[40] Results from these programs indicated that the secondary structure of Plin2 is mostly α-helical in nature (9 α-helices) with 5 β strands interconnected by random coils (Figure 1A). The Plin2 N-terminal region contains two β-strands (β1, β2) and four α-helices (α1, α2, α3, and α4). On the basis of homology to the C-terminal domain of the crystal structure of Plin3, the Plin2 C-terminal region is predicted to contain an α−β domain (α5, β3), a 4-helix bundle (α6- α9), and two β-strands (β4, β5) that together form a deep cleft that is conserved in the perilipin family and large enough to bind lipids.[25] In addition, several conserved regions have been identified within Plin2 including a highly conserved hydrophobic domain within the N-terminal region (residues 1−115) known as the PAT domain (Figure

1B), which was shown to participate in the stabilization and accumulation of lipid droplets and to determine proteasomal degradation of Plin2;[22−24] an 11-mer repeating unit of unknown function within residues 103-215 (Figure 1A); and two lipid droplet targeting domains[16,17] located in the middle and C-terminal regions (Figure 1B) that participated with part of the C-terminal domain to regulate secretion of milk lipids.[13,27] Alternating patterns of hydrophobic/hydrophilic segments are observed in Plin2 (Figure 1C) and Plin3 (Figure 1D) over the N-terminal PAT domain and 11-mer repeat region from patterns of hydrophobicity predicted using the method of Hopp and Woods.[35] In keeping with the high degree of homology shared between these proteins, similar hydrophobic characteristics were observed for both Plin2 and Plin3. Large segments of hydrophobic sequence conducive to membrane targeting were not observed with either protein, suggesting that regions within the protein come together spatially to form larger recognition surfaces for hydrophobic ligands including the membrane itself.

To assess the lipid binding affinities of these regions, Plin2 and several Plin2 deletion mutants that contain select regions within Plin2 with the potential to bind lipids were expressed in *Escherichia coli* and purified as recombinant proteins. The deletion mutants included regions containing the PAT domain,[23] one or two of the lipid droplet targeting

domains,[16,22] or the central alpha/beta domain residues near the cleft in the C-terminal region[25] (Figure 1E).

Effect of Urea and Temperature on Plin2 Structure: Intrinsic Tryptophan Fluorescence Quenching and CD Analysis. Recombinant full-length Plin2 protein was overexpressed and purified as described in the Materials and Methods section (see Supplemental Figure 1, Supporting Information). To determine if the recombinant Plin2 protein was conformational and functionally intact, two distinct experiments were performed. First, to show the effects of protein unfolding, Plin2 was titered against increasing amounts of urea, up to 6 M. Protein unfolding was monitored via tryptophan fluorescence, as described in ref 49 and in the Materials and Methods section. Tryptophan fluorescence, in contrast to tyrosine fluorescence, is sensitive to solvent polarity; therefore it can be used as a measure of protein folding.[53] Plin2 contains three tryptophan residues in the C-terminal region at positions 283, 286, and 398. More importantly, the tryptophan residues are located in the 4-helix bundle of the predicted binding region of the protein. Analysis of the Plin2 tryptophan fluorescence emission collected from 300 to 400 nm showed the refolded full-length Plin2 protein exhibited a typical emission spectra with maxima at 327 nm (Figure 2A), indicating a blue-shift relative to tryptophan in water where the fluorescence maximum is 348 nm.[55] Addition of increasing concentrations of urea (up to 6 M) resulted in fluorescence quenching of one or more of the three tryptophan residues (Figure 2A). A red-shift in the emission maxima to 332 nm at 4.6 M urea was observed, indicating increased exposure of the residues to the hydrophilic solvent. At 6 M urea, only 22% of the initial tryptophan fluorescence remained indicating substantial exposure of the tryptophan residues to the solvent. It is this 78% decrease in tryptophan fluorescence and red shift that is indicative of denaturation of the refolded protein (Figure 2B).

Second, to show the effects of protein unfolding on Plin2 secondary structure, changes in the CD spectra at increasing temperatures were examined. At room temperature (25 °C) recombinant Plin2 exhibited a double minimum at ~208 and 222 nm signifying substantial amounts of α-helices were present (Figure 2C). However, the molar ellipticity at 208 nm was lower than at 222 nm suggesting a subtle influence of random coils and β-sheets. Upon lowering the temperature to 5 °C, the minima at 208 and 222 nm were intensified, consistent with slower conformational transitions and enhanced resolution. In contrast, at 40 °C the protein began losing its secondary structure as the peak intensities approached zero molar ellipticity (Figure 2C). Results from these studies indicated that Plin2 tryptophans in the refolded protein were sensitive to urea denaturation. Moreover, CD analysis of the secondary structure of the refolded protein was consistent with predictions and exhibited enhanced resolution at lower temperatures but destabilization when temperatures were increased above room temperature.

Tryptophan Quenching Binding Studies: Full-Length Plin2 Binds Cholesterol, Stearic Acid, Arachidonic Acid, and Docosahexaenoic Acid (DHA) with High Affinity. The binding affinities of full-length Plin2 for cholesterol, stearic acid, arachidonic acid, and DHA were determined by measuring changes in the intrinsic tryptophan fluorescence of Plin2 upon ligand addition as described in the Materials and Methods section. Fluorescence quenching of one or more of the three tryptophan residues located in the C-terminal 4-helix bundle resulted in a decrease in fluorescence signal intensity when
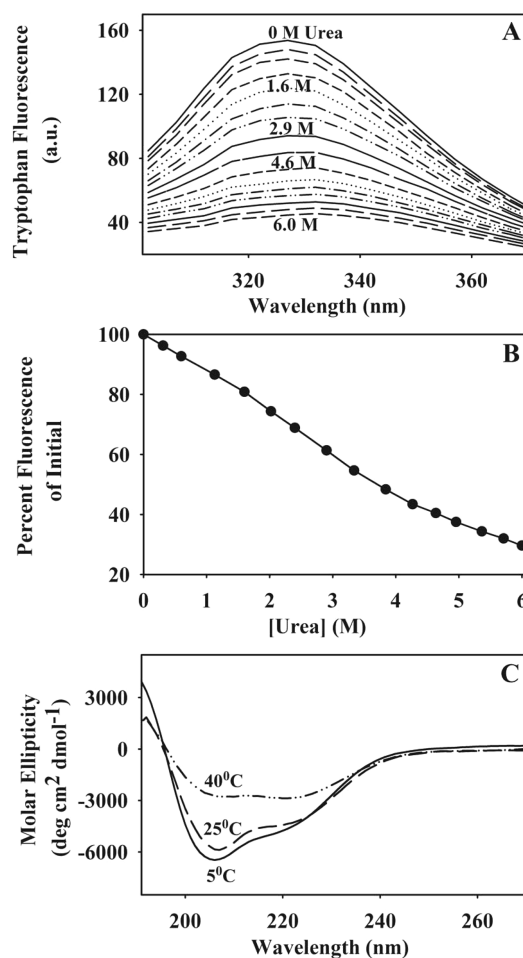

Figure 2. Tryptophan fluorescence (total and percent of initial) upon urea denaturation and circular dichroism of Plin2 as a function of temperature. Protein-denaturation studies were performed by addition of increasing aliquots of urea (0−6.0M) to recombinant Plin2. The tryptophan emission spectra (A) upon excitation at 280 nm and percent fluorescence of initial (B) was determined to show the overall effect of solvent polarity upon protein stability. Exposure of tryptophan residues to solvent upon denaturation resulted in decreased fluorescence due to quenching of residues. The effect of temperature on Plin2 secondary structure was determined by circular dichroism (C) to show Plin2 unfolding at temperatures above 40 °C.

ligand was added. It should also be noted that in some cases binding of ligand can increase tryptophan fluorescence. In situations where an increase is observed, the tryptophan residues become embedded in a hydrophobic environment either by directly interacting with the lipid residue or by a conformational change in which the reverse of tryptophan quenching occurs. Since addition of the lipid ligand was seen to cause conformational changes in Plin2, the decrease in tryptophan fluorescence upon lipid binding in the present work is thought to arise from the exposure of tryptophans to water. Saturable binding curves for cholesterol (Figure 3A), stearic acid (Figure 3B), arachidonic acid (Figure 3C), and DHA (Figure 3D) were observed and the dissociation constant K_d determined for each ligand to reveal K_d values of 7 ± 1 nM, 80 ± 9 nM, 22 ± 1 nM, and 46 ± 6 nM, respectively at a single site that was not necessarily the same for each ligand. Thus, Plin2 exhibited very high affinity for cholesterol and less so for the saturated fatty acid stearic acid, consistent with values obtained from previous studies.[5,6,8] High affinity binding was
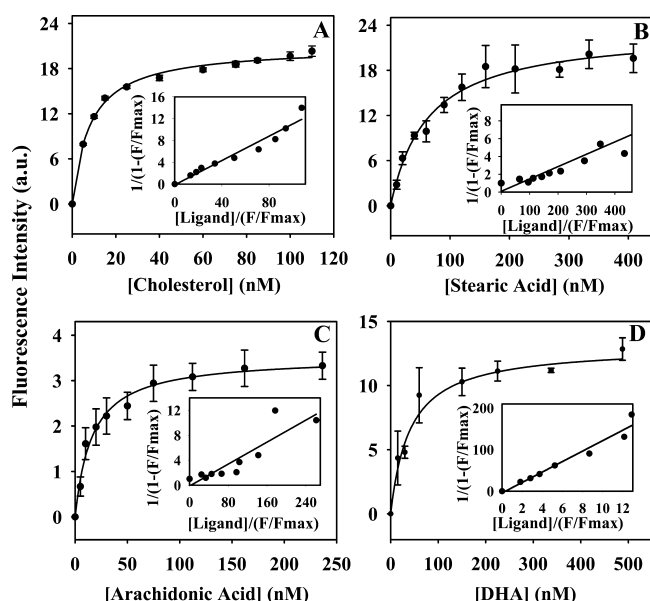
Figure 3. Tryptophan quenching binding assays. The Plin2 binding affinity for cholesterol (A), stearic acid (B), arachidonic acid (C), and DHA (D) was determined when titered with increasing amounts of ligand (1−120 nM) using a quenching of tryptophan fluorescence assay as described in the Materials and Methods. Inset, a linear plot of $1/(1 - F/F_{max})$ versus $[ligand]/(F/F_{max})$ allowed determination of the dissociation constant K_d where the slope of the line = $1/K_d$ and the ordinate intercept = nE_o/K_d and F represent fluorescence intensity at a given concentration of ligand, F_{max} is the maximal fluorescence, [ligand] is the ligand concentration, E_o is the protein concentration, and n equals the number of binding sites. Analysis of multiple curves yielded K_d of 7 ± 1 nM, 80 ± 9 nM, 22 ± 1 nM, and 46 ± 6 nM for cholesterol, stearic acid, arachidonic acid, and DHA, respectively.

also observed with the polyunsaturated fatty acids arachidonic acid (20:4n-6) and DHA (22:6n-3), indicating that the purified recombinant Plin2 protein contained an active ligand binding site for these lipids.

NBD-Labeled Binding Studies: Plin2 and Deletion Mutants Bind Cholesterol and Stearic Acid with Selective Affinity. Recombinant Plin2 deletion mutants were overexpressed and purified as described in the Materials and Methods section (see Supplemental Figure 1, Supporting Information). To establish the ability of Plin2 and the deletion mutants to bind lipids such as cholesterol and stearic acid, NBD-labeled lipid binding assays were performed as previously described.[5−8] The NBD-fluorophore in NBD-lipids was sensitive to environmental hydrophobicity and therefore provided a useful tool to determine ligand binding affinity. NBD-cholesterol showed minimal fluorescence in aqueous buffer with an emission maximum (λ_{max}) equal to 545 nm. Addition of Plin2 or the deletion mutant proteins resulted in increased fluorescence with shifts in λ_{max} to blue wavelengths (0−5 nm) indicating binding of the probe to a site increasingly more hydrophobic than the aqueous buffer (Table 1). With full-length Plin2, K_d = 11 ± 2 nM (Table 1), in keeping with results from the tryptophan quenching studies (Figure 3A) and with previous reports.[5,8] In comparison, deletion mutants Plin2-C1 (Figure 4B), Plin2-I (Figure 4F), Plin2-N2 (Figure 4E), and Plin2-C2 (Figure 4C) showed significantly less affinity for NBD-cholesterol (Table 1). Most interestingly, deletion mutant Plin2-N1 (Figure 4D) did not bind NBD-cholesterol, showing little to no increase in fluorescence over the buffer control. This

Table 1. Cholesterol and Stearic Acid Binding to Plin2 and the Deletion Mutants[a]

protein	NBD-cholesterol		NBD-stearic acid	
	K_d (nM)	λ_{max} (nm)	K_d (nM)	λ_{max} (nm)
Plin2	11 ± 2	543	121 ± 12	544
Plin2-C1	48 ± 3[b,c]	540	69 ± 7[b,c]	538
Plin2-C2	98 ± 10[b]	545	160 ± 3[b]	544
Plin2-N1	ND[d]	548	ND	545
Plin2-N2	50 ± 6[b,c]	543	92 ± 14[c]	547
Plin2-I	34 ± 4[b,c]	540	90 ± 7[c]	540

[a]The dissociation constant (K_d) and emission maximum (λ_{max}) of Plin2 and the deletion mutants for NBD-labeled cholesterol and stearic acid were determined using a fluorescent lipid binding assay as described in the Materials and Methods section. Values represent the mean ± SE (n = 3−4). [b]Indicates $P \leq 0.05$ as compared to full-length Plin2. [c]Indicates $P \leq 0.05$ as compared to Plin2-C2. [d]ND indicates no detectable binding was observed.
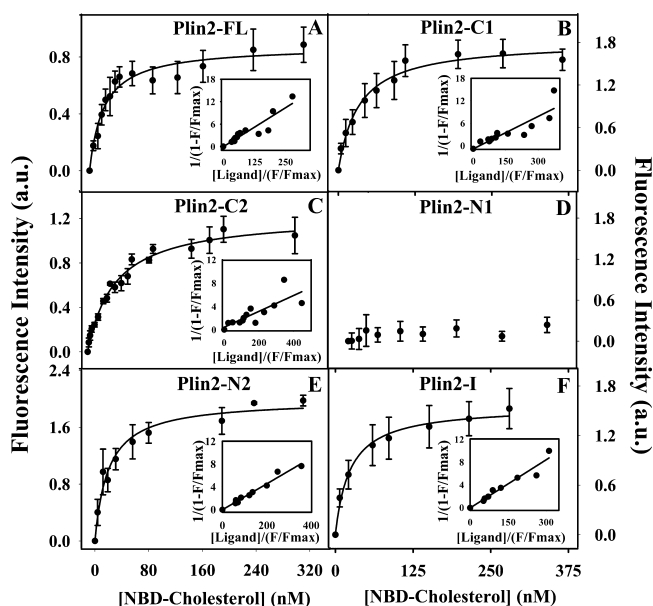

Figure 4. Titration of Plin2 and the deletion mutant proteins with NBD-cholesterol. The binding affinities of Plin2 (A), Plin2-C1 (B), Plin2-C2 (C), Plin2-N1 (D), Plin2-N2 (E), and Plin2-I (F) for NBD-cholesterol were determined using a fluorescence binding assay. The titration of the recombinant proteins with NBD-cholesterol was followed by an increase in fluorescence (excitation 480 nm, emission 540 nm). The data representing the mean ± SE of three independent measurements were fit to a single binding site model as described in Materials and Methods. Inset, a linear plot of $1/(1 - F/F_{max})$ versus $[ligand]/(F/F_{max})$ was used to determine the K_d as previously described where F represents fluorescence intensity at a given concentration of ligand, F_{max} is the maximal fluorescence, and [ligand] is the ligand concentration.

last result indicated that the cholesterol binding site for Plin2 did not reside within the PAT domain.

In a similar fashion, the full-length protein bound NBD-stearic acid with K_d = 121 ± 12 nM. These results were comparable to the higher affinity observed (K_d = 80 ± 9 nM) with unlabeled stearic acid in the tryptophan quenching study (Figure 3B). Likely, the decrease in affinity observed with the labeled ligand was due to the NBD group and its position within the binding pocket. However, despite the differences in K_d values between the labeled and unlabeled ligands, both
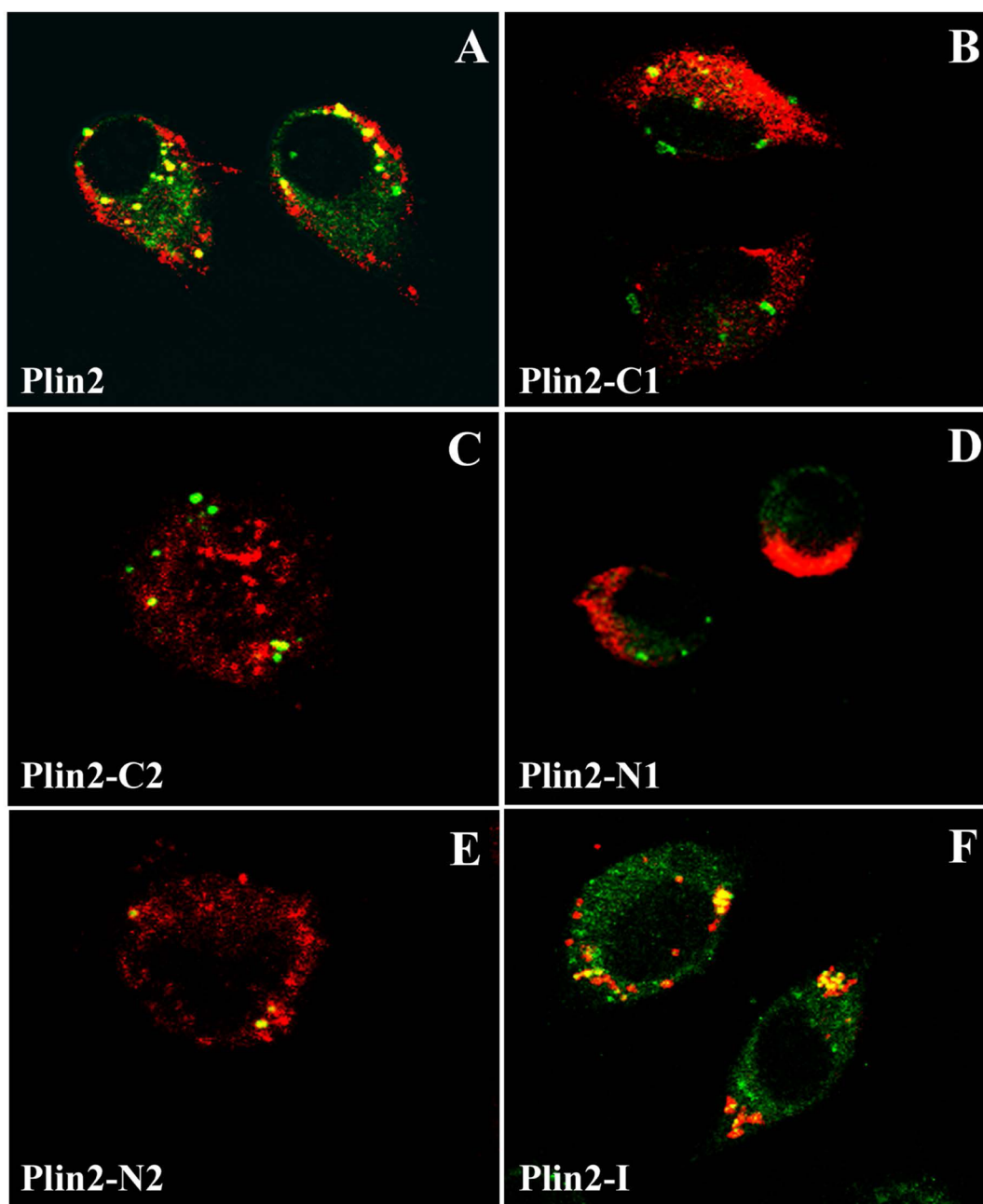
Figure 5. Confocal microscopy colocalization of NBD-cholesterol and Cy5-labeled cells expressing Plin2 and the deletion mutants. Colocalization experiments of NBD-cholesterol and Cy5-labeled L cells overexpressing Plin2 (A), Plin2-C1 (B), Plin2-C2 (C), Plin2-N1 (D), Plin2-N2 (E), or Plin2-I (F) were performed as described in the Materials and Methods section. Images were acquired sequentially and fluorescence emission was detected upon 488 nm excitation and 500/100 band path emission filter for NBD-cholesterol (green channel) and 635 nm excitation with a 725/30 band path filter for the Cy5 emission (red channel). Images derived from the red and green channels were combined and appeared as yellow to orange where superimposition of images derived from the red and green channels overlapped.

bound with affinities consistent with results from previous reports.[5,6] NBD-lipid binding studies were also performed with acyl CoA binding protein (ACBP), a cytosolic lipid binding protein that exclusively binds long-chain fatty acyl CoA[56] but not cholesterol or fatty acids.[57] When increasing concentrations of NBD-lipids were added to ACBP in solution, no increase in fluorescence was observed after background subtraction, indicating that ACBP did not bind either lipid (data not shown). These results support the specificity of Plin2 for NBD-labeled lipids.

Intracellular Targeting and FRET Analysis. The extent of Plin2/lipid interactions on the lipid droplet surface were determined in a series of experiments using NBD-labeled cholesterol in colocalization and FRET assays. First, colabeling of NBD-cholesterol with Cy5-labeled Plin2 overexpressed in L cells was accomplished as described in the Materials and Methods section and repeated with each deletion mutant. Simultaneous acquisition of multiple confocal images of NBD-cholesterol colabeled with Cy5-proteins revealed the following: (1) Plin2 (Figure 5A) and Plin2-I (Figure 5F) expression cells showed increased numbers of lipid droplets as compared to the

control (data not shown) and other mutant expression cell lines. Likewise, these expression cells showed full targeting to the lipid droplet surface. (2) Plin2-C1 (Figure 5B) and Plin2-C2 (Figure 5C) expressing cells exhibited partial targeting to lipid droplets, resulting in diminished lipid droplet number as compared to cells expressing full-length protein or Plin2-I. (3) Plin2-N2 (Figure 5E) also showed partial lipid droplet targeting but diminished number of lipid droplets as compared Plin2-C1 or -C2 expression cells. (4) In contrast, Plin2-N1 (Figure 5D) showed no targeting and the least amount of lipid droplets. These results suggested that Plin2 lipid droplet targeting was closely related to the amount of lipid droplets produced. Second, in expression clones that targeted to lipid droplets, FRET analysis was performed as described in previous work[4,52] to ascertain if the Cy5-labeled proteins and the NBD-cholesterol (ligand) are in close proximity for binding. With appropriate choice of fluorescent probes, FRET detects direct interactions at the molecular level when the donor and acceptor are in within distances of 10−100 Å. FRET was observed between NBD-cholesterol (donor) and Cy5-labeled Plin2 (acceptor) by measuring the amount of increase in donor intensity after acceptor photobleaching. The calculation of the FRET efficiency (E), a measure of the extent of probe overlap, was determined as 25 ± 5 (Table 2), values consistent with

Table 2. Intracellular Targeting and FRET Analysis of Plin2 and the Deletion Mutants in Transfected L Cells[a]

protein	intracellular targeting	E (%)	$R(R_0)$	R (Å)
Plin2	LD	25 ± 5	$1.20R_0$	67 ± 4
Plin2-C1	LD, cytosol	7 ± 1	$1.54R_0$	86 ± 4
Plin2-C2	LD, cytosol	13 ± 3	$1.37R_0$	77 ± 4
Plin2-N1	cytosol	ND	ND	ND
Plin2-N2	LD, cytosol	ND	ND	ND
Plin2-I	LD	9 ± 1	$1.47R_0$	82 ± 4

[a]Intracellular targeting, FRET efficiencies E, and distance R between Cy5-labeled Plin2 deletion proteins and NBD-cholesterol were determined as described in the Materials and Methods section. FRET was not detected (ND) in Plin2-N1 or Plin2-N2 expression cells. Values reflect mean ± SE from $n \geq 20$ lipid droplets (LD) from 20 to 30 cells. Intracellular targeting indicated localization sites of Cy5-Plin2 (red) and NBD-cholesterol (green) where yellow-to-orange indicated colocalization of the probes.

efficient overlap of electronic states and direct interaction of NBD-cholesterol and Plin2 on the lipid droplet surface. The FRET efficiency represents a mean interaction distance of $1.20R_0$. Using the calculated Förster radius, $R_0 = 56$ Å, the mean interaction distance was calculated as 67 ± 4 Å, indicating close proximity (Table 2). In a similar fashion, FRET was performed with NBD-cholesterol and the Cy5-labeled deletion mutants to show FRET occurred between the NBD-labeled ligand and the following deletion mutants: Plin2-C1, Plin2-C2, and Plin2-I with R values ranging from 85 to 96 Å (Table 2). No FRET was observed with Plin2-N1 or Plin2-N2. Taken together, these findings were consistent with results from the binding studies and indicated that Plin2 and several of the deletion mutants directly interacted with NBD-cholesterol on the lipid droplet surface.

Circular Dichroic Analysis of ADRP and Deletion Mutants. To further examine how structure affects function, the secondary structures of Plin2 and the deletion mutants were analyzed by circular dichroism (CD) both with and without

ligand (cholesterol and stearic acid). In the absence of ligand, the CD spectrum for full-length Plin2 (Figure 6A, solid line) showed a double minimum at ∼208 and 222 nm signifying the presence of substantial amounts of α-helices. The molar ellipticity was slightly lower at 208 nm than at 222 nm, however, indicating a significant amount of unordered structure or random coil. A similar trend was visible in the spectra for Plin2-N1 and Plin2-N2 before addition of ligand (Figure 6D,E, solid lines). In contrast, the CD spectra for deletion mutants Plin2-C1, Plin2-C2, and Plin2-I (Figure 6B,C,F, solid lines) showed a fairly well balanced molar ellipticity at both wavelengths along with a strong positive peak at 190−200 nm, indicating that these mutants had less unordered structure and retained strong α-helical character. These results were supported when the data were analyzed using CDSSTR software. Quantitative analysis of multiple CD spectra revealed that deletion mutants Plin2-C1, Plin2-C2, and Plin2-I exhibited the lowest proportion of unordered structure (29%, 29%, and 31%, respectively) and high α-helicity (Table 3). Similar results were shown by SELCON2 analysis (data not shown).

Further analysis of the secondary structure of Plin2 showed that Plin2 contained 21.8% α-helices and 24.5% β-strands based on analysis by CDSSTR analysis (Table 3) with similar results observed with SELCON3 analysis (data not shown). A comparison of the secondary structure of Plin2 to that of each deletion mutant showed that Plin2-C1 and Plin2-C2 had a higher percentage of α-helices (regular and distorted) than Plin2. These results were consistent with secondary structure predictions (Figure 1A) since Plin2-C1 contained the 4-helix bundle (α6, α7, α8, α9) and Plin2-C2 contained α7, α8, α9, giving them the highest α-helical percentage within the group. In contrast, the other three deletion mutants Plin2-I, Plin2-N1, and Plin2-N2 exhibited less α-helical structure than full-length Plin2 based on both methods of analysis with results showing a respective 16.4%, 10.5%, and 16.5% α-helical structure (regular and distorted). The percentage of β-sheets (regular and distorted) was also significantly higher in Plin2 (24.5%) when compared to Plin2-C1 (11.5%) and Plin2-C2 (19.1%) but significantly less than Plin2-I (30.2%), Plin2-N1 (40%), or Plin2-N2 (27.2%). Results from CDSSTR analysis showed that Plin2 had significantly more β-turns (21.8%) than Plin2-C2 (19.1%) but less than Plin2-N2 (23.4%). There were no significant differences between Plin2-C1, Plin2-I (19.3%), and Plin2-N1. In summary, in the absence of ligand, the C-terminal region of Plin2 (residues 119−436) exhibited a strong α-helical character with less unordered structure as compared to the full-length protein or mutants containing the N-terminal region (residues 1−119). Alternatively, the N-terminal region of the protein contained significantly more unordered structure than the C-terminal region.

The effect of ligand binding on secondary structure was also examined. The addition of cholesterol (Figure 6A, closed circles) and stearic acid (Figure 6A, open circles) altered the shape of the CD spectrum of full-length Plin2, intensifying the minima at 208 nm with cholesterol but diminishing the peak when stearic acid was present. These alterations were reflected by significant changes in the percent composition of α-helical structures where an increase and decrease respectively was observed when cholesterol and stearic acid were added to the protein. With the deletion mutants, subtle changes in the CD spectra were also observed upon addition of ligands. As with the full-length protein, the CD spectrum of Plin2-C1 showed a significant increase in the intensity of the 208 nm minimum
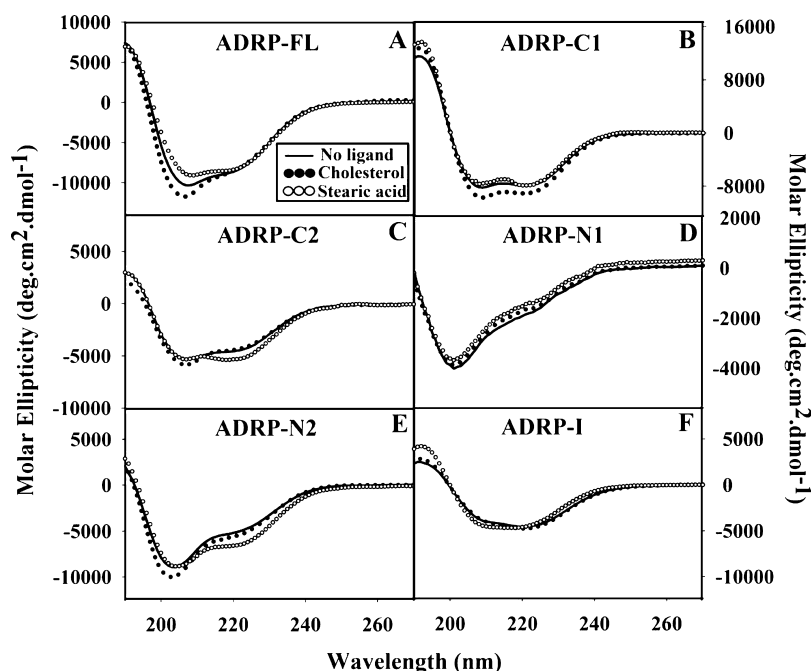
Figure 6. Circular dichroic analysis of Plin2 and the deletion mutants. Far ultraviolet (UV) circular dichroic (CD) spectra of Plin2 (A), Plin2-C1 (B), Plin2-C2 (C), Plin2-N1 (D), Plin2-N2 (E), and Plin2-I (F) was shown in the presence or absence of ligand (cholesterol or stearic acid, 5 μM). Solid line indicates protein without ligand. Spectral trace designated by closed circles indicates protein incubated with cholesterol; open circle indicates protein incubated with stearic acid. Each spectrum represents an average of 10 scans repeated in triplicate.

Table 3. Predicted Secondary Structures of Plin2 and the Deletion Mutants in the Presence and Absence of Cholesterol and Stearic Acid[a]

		secondary structure (%)					
		H(r)	H(d)	S(r)	S(d)	turns	unrd
Plin2	(−)Ligand	10.3 ± 0.1	11.5 ± 0.2	15.0 ± 0.1	9.5 ± 0.1	21.8 ± 0.1	31.7 ± 0.1
	(+)Chol	12.05 ± 0.4**	11.7 ± 0.3	15.3 ± 0.1	9.4 ± 0.1	21.5 ± 0.4	31.1 ± 0.2
	(+)STA	9.9 ± 0.1**	11.1 ± 0.2	15.0 ± 0.3	9.9 ± 0.1**	21.9 ± 0.1	32.2 ± 0.2
Plin2-C1	(−)Ligand	21.3 ± 0.2*	19.6 ± 0.6*	6.1 ± 0.6*	5.4 ± 0.4*	19.1 ± 1	28.0 ± 0.5*
	(+)Chol	27.7 ± 0.2**	23.6 ± 0.2**	5.0 ± 0.1	4.9 ± 0.1	18.2 ± 0.2	26.9 ± 0.2
	(+)STA	18.3 ± 0.2**	18.3 ± 0.2	7.0 ± 0.6	6.5 ± 0.1	20.9 ± 0.8	29.2 ± 0.4
Plin2-C2	(−)Ligand	18.6 ± 0.1*	14.2 ± 0.1*	11.2 ± 0.1*	7.9 ± 0.1*	19.1 ± 0.1*	29.1 ± 0.1*
	(+)Chol	19.6 ± 0.4	13.4 ± 0.1**	11.3 ± 0.7	8.1 ± 0.1	19.1 ± 0.5	29.7 ± 0.2
	(+)STA	18.8 ± 0.1	14.1 ± 0.1	11.3 ± 0.1	8.0 ± 0.1	19.0 ± 0.2	28.6 ± 0.1**
Plin2-I	(−)Ligand	7.5 ± 0.2*	8.9 ± 0.1*	19.0 ± 0.2*	11.2 ± 0.1*	21.9 ± 0.1	30.6 ± 0.1*
	(+)Chol	6.3 ± 0.1**	9.1 ± 0.1	19.4 ± 0.1	11.2 ± 0.1	21.8 ± 0.1	30.9 ± 0.2
	(+)STA	6.9 ± 0.1	8.5 ± 0.1**	19.9 ± 0.1**	11.6 ± 0.1**	22.1 ± 0.1	30.3 ± 0.1
Plin2-N1	(−)Ligand	0.8 ± 0.5*	2.5 ± 0.8*	26 ± 3*	14 ± 1*	27 ± 2	30 ± 4
	(+)Chol	0.4 ± 0.1	3.8 ± 0.2	26.5 ± 0.7	12.5 ± 0.1	22.1 ± 0.6	33.8 ± 0.2
	(+)STA	0.1 ± 0.1	3.6 ± 0.4	25.7 ± 0.2	12.4 ± 0.1	24 ± 1	32 ± 1
Plin2-N2	(−)Ligand	6.5 ± 0.1*	10.0 ± 0.2*	16.5 ± 0.1*	10.7 ± 0.1*	23.4 ± 0.1*	33.0 ± 0.2*
	(+)Chol	5.2 ± 0.4**	7.1 ± 0.4**	18.1 ± 0.3**	11.0 ± 0.2	23 ± 1	33 ± 1
	(+)STA	6.9 ± 0.2	10.4 ± 0.1	16.1 ± 0.1**	10.6 ± 0.1	23.5 ± 0.2	32.6 ± 0.2

[a]All conditions were as described in the Materials and Methods section. Values represent the mean ± SE (10 iterations/run performed in triplicate) analyzed by CDSSTR. H(r) indicates regular α-helices; H(d), distorted α-helices; S(r), regular β-sheets; S(d), distorted β-sheets; Unrd, unordered structures. Chol refers to cholesterol and STA to stearic acid. (*) indicates $P \leq 0.05$ as compared to Plin2 without ligand. (**) indicates $P \leq 0.05$ as compared to each protein in the absence of ligand.

when cholesterol was added but a significant decrease upon addition of stearic acid, reflecting significant increases in both disordered helices and unordered structures while decreasing the percentage of β-sheets (Figure 6B, Table 3). Subtle conformational changes in the CD spectra were also observed with Plin2-C2, Plin2-I, and Plin2-N2 upon ligand addition, reflecting significant changes in percentage of α-helices and β-

sheets based on CDSSTR analysis (Table 3). All three mutants exhibited significant decreases in α-helical structure when cholesterol was added, concomitant with significant increases in β-sheet and unordered structure (Table 3). In summary, the CD results were consistent with the predicted secondary structure (Figure 1) and indicated that several of the proteins were sensitive to ligand binding. Lack of conformational change

upon ligand binding with deletion mutant Plin2-N1 was consistent with results from the binding studies which indicated that this mutant did not bind cholesterol or stearic acid. Interestingly, the decrease in signal, along with the increase in unordered structure upon addition of stearate, was indicative of a more flexible binding pocket that does not enhance the secondary structure of Plin2. Conversely, addition of cholesterol enhanced CD signal and increased the percentage of α-helical character. This increase in structured secondary structure suggests that binding of cholesterol was dependent on a defined secondary structure.

The Tertiary Structure of the Plin2 C-Terminal Domain Defines a Cleft That Can Interact Favorably with Stearic Acid and Cholesterol. The tertiary structure of Plin2 (Figure 7A) was modeled by using two comparative modeling approaches. Homology modeling by Modeler[42] (web server: http://salilab.org/modweb) was employed for the C-terminal domain based on its sequence similarity to Plin3, since this technique provides the most accurate structural models. Modeler constructed a homology model of the structure of C-terminal residues 190−409 of murine Plin2 (Figure 7A) based on its alignment with murine Plin3 (also known as TIP47) with 38% sequence identity, well above the 25% threshold required for confident homology modeling.[28] In the absence of a structural template with high enough sequence similarity to the N-terminal region of Plin2 to allow homology modeling, the next most accurate approach, fold recognition, was used. This approach defines the best-matching structural template in the Protein Data Bank (PDB) based on the compatibility of the query sequence with the primary and secondary structure of the NMR or crystal structure being evaluated as a template, and the favorability of the 3-dimensional chemical interactions of each residue with its neighbors when modeled using that particular 3-D structure. The Pcons.net (http://pcons.net) server was used to model residues 1−171 of murine Plin2 based on the consensus of predicted structures from 11 different fold recognition methods. Of the 10 highest-consensus structural models provided by Pcons, two corresponded to functionally relevant apolipoprotein structures that form compact α-helical bundles: apolipophorin III (PDB entry 1AEP, residues A6−A158);[58] and apoliprotein A-I (PDB entry 2A01, residues A44-A187).[59] The apolipophorin-based model for Plin2 was chosen based on having higher sequence identity (20%, relative to 10% sequence identity for apolipoprotein A-I). Additionally, the matched region of Plin2 corresponds to the entire helical bundle structure of apolipophorin, including a fifth, irregular helix, as shown in yellow in Figure 7A. This model is consistent with previous studies suggesting N-terminal domain homology with apolipoproteins.[25,27] Together, the N-terminal apolipo-phorin (left side of Figure 7A) and C-terminal Plin3-based structural model (right side of Figure 7A) cover all but the 18 linking residues between the two domains and the 16 C-terminal residues of Plin2, which could not be modeled due to lack of homology. A close sequence match in the PDB was found for 13 of the 18 linking residues in Plin2 (VDNAITK-SELLVD) which match residues A136−A153 in PDB entry 1E6B (VNNAITKGFTALEKLLVN), forming an α helix.[60] The central residues FTAL in this known structure are an insertion corresponding to a full turn of helix not found in the Plin2 sequence. Though the matching sequence comes from a glutathione S-transferase, which is unlikely to be a functional homologue of Plin2, an exact match of 9/13 residues between these two peptides means they are statistically likely to fold the
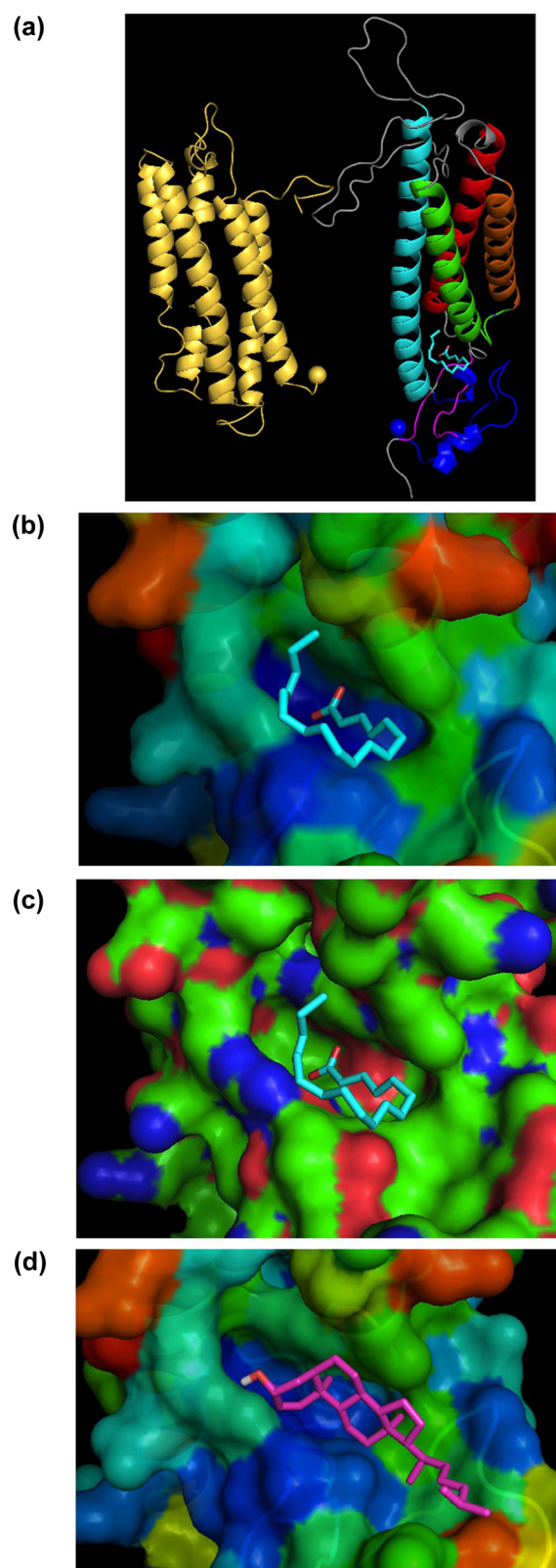

(a)

(b)

(c)

(d)

Figure 7. Plin2 has an apophorin-like N-terminal domain and a Plin3-like C-terminal domain containing a potential lipid binding cleft. The N-terminal domain structure of Plin2 (residues 1−171; shown in yellow ribbons) was modeled using the *n*-fold fold recognition server via Pcons, based on the high degree of Plin2 sequence and secondary structural compatibility with the three-dimensional structure of apolipophorin III (PDB entry 1AEP), and this model's consensus with the top-scoring results from 11 other fold recognition predictions

Figure 7. continued

for the N-terminal Plin2 sequence, all of which are α-helical bundles. This structure contains five helices connected by turns in a compact bundle. This model for the N-terminal 171 residues of Plin2 received a Pcons consensus score of 0.77, indicating a high degree of shared features with the top-scoring models from the different fold recognition methods. A value of 0.77 corresponds to 98% sensitivity (meaning 98% of the proteins of similar fold are predicted correctly) and 94% specificity (meaning that 94% of proteins with dissimilar folds will not be incorrectly assigned as similar in fold). The homology model of the C-terminal domain of Plin2 appears to the right in panel (a), based on its 38% sequence identity with the crystal structure of the corresponding region in Plin3 (residues 191–437, PDB entry 1SZI). The structure contains a 4-helix bundle (cyan, green, orange, and red helices), which together with an α–β domain (blue, magenta, and light gray) form the cleft. Stearic acid (the U-shaped light blue-colored stick figure, with carboxylate oxygens in red) is shown positioned in this cleft, based on the most energetically favorable binding mode predicted by SLIDE.[48] Cleft residues include Val203, Tyr215, Ala233, Arg236, Val237, Ala240, Thr325, Val326, Asn329, Gln331, Trp398, Leu399, Val400, Pro402, and Phe403. (b) ConSurf analysis of residue conservation in the perilipin family, color-mapped onto the surface of the Plin2 C-terminal domain. The position of the cleft is indicated by the predicted binding mode for stearic acid (light blue stick figure). Dark blue to green surface indicates the most highly and next most highly conserved residues in perilipins mapped onto the Plin2 structure, and yellow to red indicate increasingly low conservation. (c) Atom-colored surface representation of the same region in Plin2 (green for carbon, blue for nitrogen, and red for oxygen atoms). Hydrogen-bonding atoms are found deep in the cleft ringed by hydrophobic surface, positioned such that they can bridge to the predicted position of the carboxylate group in stearic acid. (d) Predicted most favorable mode of cholesterol binding (pink tubes) with the conserved cleft of Plin2, shown with surface colored by residue conservation (as in panel B, above).

same, as an α helix as previously described.[28] Thus, the C-terminus (yellow sphere at bottom center of Figure 7a) of the apolipophorin-like domain and the N-terminus (blue sphere) of the Plin3 domain may well be connected by a helical linker. The model presented here is consistent with the solution based structures for Plin3 described by Hynson et al., who show the Plin3 C-terminal domain as one-half of an elongated structure.[31] Their volumetric profile is consistent with end-to-end packing of the N-terminal and C-terminal domains in the Plin3 solution structure.

ConSurf multiple-sequence alignment of 38 diverse proteins in the Plin family yielded conservation values for each residue, which were color-mapped onto the surface of the Plin2 C-terminal domain structure and defined a cleft region (Figure 7b). In the model, blue identified highly conserved residues with a gradient toward green, yellow, orange and red indicating decreasing chemical conservation. The Plin2 model was also colored by atom type, with blue for nitrogen atoms, green for carbon, and red for oxygen atoms (Figure 7c). In both models the most favorable mode of stearic acid interaction with the cleft was predicted by SLIDE molecular docking[48] to reveal 5613 favorable conformers of stearic acid generated by Omega2, including protein side-chain and ligand single-bond rotations for steric complementarity between stearic acid and Plin2. The result was an orientation of stearic acid and conformation of Plin2 side chains that yielded a favorable predicted $\Delta G_{binding}$ (−7.5 kcal/mol). The resulting orientation of stearic acid matches a highly conserved surface patch in Plin2

(blue region, Figure 7b), as well as placing the terminal carboxylate group of stearic acid within favorable distance of conserved hydrogen-bonding groups, including the Arg236 guanidinium on helix α6, the side-chain amines of Asn329 (helix α6) and Trp398 (β4), and the main-chain nitrogen of Gly401 (β4), all absolutely conserved between Plin2 and Plin3. Since some of the deletion mutants (e.g., Plin2-N2 or Plin2-C2) remove several residues contributing to the cleft, the stearic acid binding orientation would likely differ in those cases. In fact, Plin2-C2 most likely retains lipid binding ability despite the lack of key structural features of the cleft domain (helix α4, the α–β domain, and part of helix α6) due to retention of interacting residues including Asn329, Trp398 (β4), and Gly401. Docking of cholesterol into the same cleft (Figure 7d) resulted in greater predicted affinity of binding (−9.6 kcal/mol) relative to steric acid. Cholesterol formed interactions with several residues including Val205, Phe208, Val211, the aliphatic part of Lys213, and Tyr217 in the α–β domain, Thr325 and Val328 in helix α7, and Pro402 in strand β4. Hydrophobic contacts were also made with the collar region created by the conserved residues identified in Plin3.[25] Since these residues are conserved between Plin2 and Plin3, similar lipid interactions are also possible in Plin3.

■ DISCUSSION

Previous studies demonstrated that Plin2 binds lipids with high affinity[4−8] and is involved in lipid droplet formation,[1] triacylglycerol accumulation,[1−4] fatty acid uptake,[9] and lipoprotein regulation.[8,12] Despite these findings, little is known regarding the structural and functional requirements of Plin2−lipid interactions that facilitate these processes. To address this issue, truncated Plin2 mutants were designed to contain one or more predicted domains conserved among the Plin protein family to identify structural motifs required for Plin2 lipid binding. Studies herein provide the following new insights. First, the N-terminal PAT domain is not involved in lipid binding since the Plin2-N1 mutant (containing the PAT domain) showed no evidence of binding lipids. These results are consistent with earlier studies that give evidence that the PAT domain is involved in other roles including lipid droplet stabilization, lipid accumulation, and proteasomal degradation of Plin2.[24] Second, Plin2 residues 119−251, containing helix α4, the α−β domain, and part of helix α6 form a Plin3-like cleft found to be important for highest affinity lipid binding. This follows from findings that mutants containing residues 119−251 (Plin2-C1 and Plin2-N2) showed the highest affinity for cholesterol and stearic acid ligands, while those lacking these residues exhibited the least (Plin2-C2) or no (Plin2-N1) lipid binding. With Plin2-C2, NBD-stearate and NBD-cholesterol binding decreased up to 9-fold when compared to the full-length protein and more than 3-fold when compared to Plin2-C1, resulting in a protein that still targeted to lipid droplets but with the lowest affinity of all the mutants that showed binding. Results finding residues 119−251 important to binding are not surprising, since the region includes structures found in the X-ray crystal of Plin3 that form a cleft of sufficient size to accommodate lipid ligands.[25] In addition, other work shows that the region of Plin2 within residues 119−426 is able to fold and function independently from the rest of the protein.[27] Some of the residues within the cleft region, however, are not entirely essential for lipid binding since removal of the α−β domain (residues 171−219) resulted in a mutant (Plin2-I) with similar binding affinity to that of the full-length protein. It

should also be noted that affinities for the two ligands (cholesterol and stearic acid) were distinctly different. For example, Plin2-I showed a 3-fold decrease in NBD-cholesterol binding as compared to the full-length protein, but with NBD-stearic acid no significant change in binding was observed. The results suggest that Plin2 has slightly different determinants for cholesterol and stearic acid binding. For instance, the proposed lipid binding site in the C-terminal domain (Figure 7) has some shared interactions for cholesterol and stearic acid binding, but different footprints due to the different chemical structures of the individual ligands. Consistent with this, Plin2 is known to support binding to an array of lipids with diverse structures such as phospholipids, sphingomyelin, cholesterol, and fatty acids.[5−8] In the present study, we show for the first time that Plin2 binds polyunsaturated fatty acids including arachidonic acid, a ω6 fatty acid that is precursor to several families of pro-inflammatory eicosanoid lipid mediators, and DHA, a ω3 fatty acid associated with anti-inflammatory benefits, with high affinity (K_d = 22 ± 1 nM and 46 ± 6 nM, respectively). These results suggest that lipid droplets may act as physiological stores for essential fatty acids. In addition, since Plin2 binds arachidonic acid with 2.1-fold higher affinity than DHA and close to 4-fold higher affinity than stearic acid, these findings support Plin2 selectively sequestering proinflammatory fatty acids to the lipid droplet surface. Consistent with this, arachidonic acid-derived eicosanoids have been detected on lipid droplets that colocalize with Plin2.

Discrete targeting of the Plin2 mutants to lipid droplets was also demonstrated. Deletion mutants Plin2-N1, containing residues 1−119 (the PAT domain) and Plin2-N2, comprised of residues 1−251 (the PAT domain, helix α4, α5-β3 domain, part of helix α6) did not target to lipid droplets or show FRET interactions, consistent with earlier work demonstrating that N-terminal deletion mutants containing residues 1−131 were not found on lipid droplets.[16,17] Addition of 52 residues to the PAT domain salvaged targeting ability in previous studies,[16,17] suggesting the presence of a lipid droplet targeting domain in the central region of the protein. With regard to C-terminal mutants, both Plin2-C1 (containing residues 119−426) and Plin2-C2 (residues 251−426) targeted to lipid droplets, consistent with previous reports.[16,17] However, removal of residues 154−174 in other studies[16] showed lack of targeting, while exclusion of residues 172−218 in the present work resulted in a protein that targeted lipid droplets and interacted with NBD-cholesterol in FRET assays. Despite some inconsistencies between reports, these results reinforce the idea that Plin2 contains two independent, nonoverlapping targeting domains in its internal and C-terminal sequence that need consideration of the tertiary structure to understand their structure. Likewise, the fluorescence binding data supported that the ligand binding site of Plin2 is not dictated by a linear structural motif within the primary sequence. Much like the regions required for lipid droplet targeting, domains involved in forming the lipid binding pocket of the protein come from noncontiguous parts of the protein. This motivated the modeling of Plin2 tertiary structure to understand how these regions organize into functional lipid binding and targeting domains. The tertiary structure of Plin2 was modeled using Modeler and Pcons, also providing insights into the differences in ligand binding affinities among the mutant proteins. Comparative modeling revealed the Plin2 tertiary structure contained an apolipophorin III-like N-terminal domain and a TIP47-like C-terminal domain, which were linked by 18

residues. Consistent with earlier predictions and X-ray crystal data for the most similar proteins, the modeled N-terminal domain is likely to form an α-helical bundle,[26,27] while the C-terminal domain contained a highly conserved cleft formed from the union of the α−β domain and the 4-helix bundle with high homology to the corresponding crystal structure of this region in Plin3.[25] ConSurf multiple-sequence alignment identified highly conserved residues within the Plin family which localize to the cleft. SLIDE molecular docking[48] revealed favorable conformers of stearic acid and cholesterol interaction in the cleft region. Key residues predicted to interact with stearic acid included Trp398, Gly401, and two residues in helix α6, Arg236 and Asn329 that are conserved between Plin2 and Plin3, suggesting conservation of function. Cholesterol formed interactions with several residues in the same region as stearic acid including Val205, Phe208, Val211, Lys213, and Tyr217. However, cholesterol also interacted with residues Thr325 and Val328 in helix α7, and Pro402 in strand β4 near the C-terminal end of the protein. Orientations of stearic acid and cholesterol within the cleft were favored energetically, with cholesterol predicted to have greater affinity of binding relative to stearic acid ($\Delta G_{binding}$ of −9.6 kcal/mol versus −7.5 kcal/mol). These results were consistent with experimental binding results that showed Plin2 bound NBD-cholesterol with higher affinity than NBD-stearic acid. Deletion mutants that remove residues contributing to the cleft (e.g., Plin2-I) would also be expected to differ in binding interactions and affinity, as was observed with the experimental data demonstrating higher affinity for stearic acid than cholesterol with deletion mutant Plin2-I and decreased affinity for cholesterol when compared to the full-length protein. Moreover, Plin2-C2 is missing some structures that form the cleft domain but retention of several interacting residues (Asn329, Trp398, Gly401, Thr325, Val328, and Pro402) likely contributes to its ability to bind both stearic acid and cholesterol, although at decreased affinity. These results support that the predicted cleft in the C-terminal region of Plin2 favorably binds lipids.

Structural changes induced by mutation or ligand addition were also examined. Plin2 in the absence of ligand was significantly helical. However, the percentage of helical content doubled in the Plin-C1 and Plin-C2 mutants, in which the N-terminal domain and part or all of the α−β domain were absent, suggesting that the C-terminal region is much more strongly helical than the N-terminal region. These trends were preserved in the presence of both cholesterol and stearic acid, suggesting that ligand binding does not dissolve or nucleate helical structure in Plin2. Consistent with these findings, Hynson et al. showed that the C-terminal region of the homologous Plin3 protein was mostly α-helical with little β-strand content.[31] In addition, the Plin3 N-terminal was found to increase the percentage of amino acid residues forming β-strand, turns, and random coil.[31] CD analysis of the Plin2 N-terminal region showed similar results, despite the sequence-based prediction of predominantly helical structure for the N-terminal half of the protein. One interpretation of these results is that the N-terminal helices are less stable and fluctuate more without the presence of lipid ligand or membrane. Indeed, studies with the Plin3 protein show the N-terminal region is highly elongated in solution, suggesting that Plin3 N-terminus becomes a highly structured domain upon interaction with lipids or membrane.[31] However, the Plin2 N-terminal domain may interact differently, and these domain orientations could also change when associated with a lipid droplet. It should be

noted that conformational change in another lipid droplet protein, Plin1 occurs upon hyperphosphorylation, allowing access to lipids in the droplet.[61−64] This raises the question as to whether the C-terminal domain of Plin2, containing the suggested binding site for stearic acid and cholesterol, is likely to undergo a large-scale rearrangement upon interacting with lipid droplets. Amphipathic α-helical bundles with tightly packed hydrophobic cores, like that found in Plin2, are not typically observed to alter conformation significantly due to the considerable energy it would take to disrupt the extensive favorable hydrophobic interactions within the core. Even the highly hydrophobic helical bundles in integral membrane proteins like cytochrome c oxidase typically only show coupled motion of helices rather than any reorganization of interfaces.[65] Viral fusion with host membranes has been shown in some cases to depend on the formation of helical bundles as a rate-limiting step.[66] The same phenomenon has been observed for Hsp12 stress proteins, which are unfolded in the cytosol and then adopt helical conformation upon interaction with the membrane.[67] Because the helical bundles in Plin2 have polar surfaces, however, it is hard to imagine any configuration or rearrangement in which they could be favorably buried inside a lipid milieu. Thus, association could be with the surface of the lipid droplet, through interaction with polar headgroups, or by a tethering mechanism. Indeed this was shown through a series of experiments by McManaman et al. in which the polar surface of the helical bundles targeted to membranes in nonionic solutions and were displaced as salt was added.[27] These results further support that the 4-helix bundle in the C-terminus of Plin2 can interact with polar headgroups of the lipid droplet thereby binding and sequestering lipids.

Lipid droplet targeting was also associated with maintenance of the helical regions in both the N- and C-terminal helical bundles, as evidenced by Plin2 and Plin2-I being fully targeted to lipid droplets, while the other mutants were partially or fully targeted to the cytoplasm. Fluorescence binding and FRET results with labeled cholesterol support strong interactions between cholesterol and the native Plin2 structure, with weaker interactions with Plin2-C1, Plin2-C2, Plin2-I, and Plin2-N2 constructs. No evidence for cholesterol (or stearic acid) interaction with Plin2-N1 was detected. These results support the crucial role of the C-terminal helical bundle region of Plin2 that is homologous to Plin3 for binding lipids; this region contains the conserved cleft. Other recent reports support the functional importance of the Plin family's C-terminal regions.[68,69] The C-terminal region of Plin1 contains a C-terminal region, implicated in binding AB-hydrolase domain containing-5 (ABHD5), a cofactor that prevents the activation of adipose tissue triacylglycerol lipase. Patel et al.[68] demonstrated that fusing the carboxy terminal region of Plin1 to the amino terminus of Plin2 was sufficient to stabilize ABHD5 and suppress basal lipolysis. For Plin5, Sztalryd et al.[69] demonstrated that fusing the carboxy terminal region of Plin5 to Plin2 generated a protein that was able to recruit lipid droplets to mitochondria, whereas Plin2 by itself did not. Our work supports specific lipid binding as a function for the C-terminal region in Plin2.

In summary, the modeled tertiary structure for Plin2 highlighted the structural and functional features necessary for ligand binding and lipid droplet targeting. The PAT domain was not required for lipid binding or lipid droplet targeting; removal of this domain resulted in C-terminal mutants with high affinity for lipids. Crucial elements contained within residues 119−251 in the C-terminal region include the central α−β domain, along with the conserved end of helix α6, which form part of the cleft region. Removal of these residues decreased binding with cholesterol and stearic acid ligands several-fold. Evidence of the functional relevance of this region was recently provided in studies with a human Plin2 variant where a serine to proline mutation at residue 251 caused individuals with the minor allele to exhibit decreased plasma triglyceride and decreased VLDL levels.[12] Structurally, the mutation would be predicted to disrupt helix α6. In the present work, both cholesterol and stearic acid were shown through molecular docking experiments to interact favorably with a cleft formed by conserved residues within the C-terminal region, including helix α6. Furthermore, the modeled interactions together with the mutant construct binding studies suggest that this conserved cleft is a site of favorable lipid interaction for both cholesterol and stearic acid.

■ ASSOCIATED CONTENT

ⓢ Supporting Information

Purification of recombinant Plin2 and deletion mutants. This material is available free of charge via the Internet at http://pubs.acs.org.

■ AUTHOR INFORMATION

Corresponding Author

*Telephone: (517) 353-5284. Fax: (517) 353-9334. E-mail: atshaves@msu.edu.

Author Contributions

#C.P.N. and J.S.L. contributed equally to the development of this manuscript.

Notes

The authors declare no competing financial interest.

■ ACKNOWLEDGMENTS

■ ABBREVIATIONS:

Plin, perilipin; ADRP, adipose differentiation-related protein; TIP47, tail-interacting protein 47; PAT, perilipin/ADRP/TIP47; ACBP, acylCoA binding protein; NBD-cholesterol, [22-(N-(7-nitrobenz-2-oxa-1,3-diazol-4-yl)amino)-23,24-bis-nor-5-cholen-3b-ol]; NBD-stearate, 12-N-methyl-(7-nitrobenz-2-oxa-1,3-diazo)aminostearic acid; PDB, Protein Data Bank; HDL, high density lipoproteins; VLDL, very low density lipoproteins; and FRET, fluorescence resonance energy transfer

■ REFERENCES

(1) Fukushima, M., Enjoji, M., Kohjima, M., Sugimoto, R., Ohta, S., Kotoh, K., Kuniyoshi, M., Kobayashi, K., Imamura, M., Inoguchi, T., Nakamuta, M., and Nawata, H. (2005) Adipose differentiation related

protein induces lipid accumulation and lipid droplet formation in hepatic stellate cells. *In Vitro Cell Dev. Biol. Anim. 41*, 321−324.

(2) Larigauderie, G., Cuaz-Perolin, C., Younes, A. B., Furman, C., Lasselin, C., Copin, C., Jaye, M., Fuchart, J. C., and Rouis, M. (2006) Adipophilin increases triglyceride storage in human macrophages by simulation of biosynthesis and inhibition of beta-oxidation. *FEBS J. 273*, 3498−3510.

(3) Listenberger, L. L., Ostermeyer-Fay, A. G., Goldberg, E. B., Brown, W. J., and Brown, D. A. (2007) Adipocyte differentiation-related protein reduces the lipid droplet association of adipose triglyceride lipase and slows triacyglycerol turnover. *J. Lipid Res. 48*, 2751−2761.

(4) McIntosh, A. L., Senthivinayagam, S., Moon, K. C., Gupta, S., Lwande, J. S., Murphy, C. C., Storey, S., and Atshaves, B. P. (2012) Direct interaction of ADRP with lipids on the surface of lipid droplets: A live cell FRET analysis. *Am. J. Physiol. Cell Physiol. 303*, C728−742.

(5) Serrero, G., Frolov, A., Schroeder, F., Tanaka, K., and Gelhaar, L. (2000) Adipose differentiation related protein. Expression, purification of recombinant protein in E. coli and characterization of its fatty acid binding properties. *Biochim. Biophys. Acta 1488*, 245−254.

(6) Atshaves, B. P., Storey, S. M., McIntosh, A. L., Peterscu, A. D., Lyuksyutova, O. I., Greenberg, A. S., and Schroeder, F. (2001) Sterol carrier protein 2 expression modulates protein and lipid composition of lipid droplets. *J. Biol. Chem. 276*, 25324−25335.

(7) McIntosh, A. L., Storey, S. M., and Atshaves, B. P. (2010) Intracellular lipid droplets contain dynamic pools of sphingomyelin: ADRP binds phopholipids with high affinity. *Lipids 45*, 465−477.

(8) Frolov, A., Petrescu, A., Atshaves, B. P., So, P. T. C., Gratton, E., Serrero, G., and Schroeder, F. (2000) High density lipoprotein mediated cholesterol uptake and targeting to lipid droplets in intact L-cell fibroblasts. *J. Biol. Chem. 275*, 12769−12780.

(9) Gao, J., and Serrero, G. (1999) Adipose differentiation related protein (ADRP) expressed in transfected COS-7 cells selectively stimulates long chain fatty acid uptake. *J. Biol. Chem. 274*, 16825−16830.

(10) Atshaves, B. P., Starodub, O., McIntosh, A. L., Roths, J. B., Kier, A. B., and Schroeder, F. (2000) Sterol carrier protein-2 alters HDL-mediated cholesterol efflux. *J. Biol. Chem. 275*, 36852−36861.

(11) Chang, B. H., Li, L., Saha, P., and Chan, L. (2010) Absence of adipose differentiation related protein upregulates hepatic VLDL secretion, relieves hepatosteatosis, and improves whole body insulin resistance in leptin-deficient mice. *J. Lipid Res. 51*, 2132−2142.

(12) Magne, J., Aminoff, A., Sundelin, J., Mannila, M. N., Gustafsson, P., Hultenby, K., Wernerson, A., Bauer, G., Listenberger, L. L., Neville, M., Karpe, F., Boren, J., and Ehrenborg, E. (2013) The minor allele of the missense polymorphism Ser251Pro in perilipin 2 (PLIN2) disrupts an α-helix, affect lipolysis, and is associated with reduced plasma tryglyceride concentration in humans. *FASEB J. 27*, 3090−3099.

(13) Brasaemle, D. L., Subramanian, V., Garcia, A., Marcinkiewicz, A., and Rothenberg, A. (2009) Perilipin A and the control of triacylglycerol metabolism. *Mol. Cell. Biochem. 326*, 15−21.

(14) Subramanian, V., Garcia, A., Sekowski, A., and Brasaemle, D. L. (2004) Hydrophobic sequences target and anchor perilipin A to lipid droplets. *J. Lipid Res. 45*, 1983−1991.

(15) Fujimoto, T., Kogo, H., Ishiguro, K., Tauchi, K., and Nomura, R. (2001) Caveolin-2 is targeted to lipid droplets, a new membrane domain in the cell. *J. Cell. Biol. 152*, 1079−1085.

(16) Nakamura, N., and Fujimoto, T. (2003) Adipose differentiation-related protein has two independent domains for targeting to lipid droplets. *Biochem. Biophys. Res. Commun. 306*, 333−338.

(17) Targett-Adams, P., Chambers, D., Gledhill, S., Hope, R. G., Coy, J. F., Girod, A., and McLauchlan, J. (2003) Live cell analysis and targeting of the lipid droplet-binding adipocyte differentiation-related protein. *J. Biol. Chem. 278*, 15998−16007.

(18) Wiener, M. (2005) A census of ordered lipids and detergents in X-ray crystal structures of integral membrane proteins, In *Protein-Lipid Interactions: From Membrane Domains to Cellular Networks* (Tamm, L., Ed.) Wiley-VCH Verlag GmbH & Co, New York.

(19) Qin, L., Sharpe, M., Garavito, R., and Ferguson-Miller, S. (2007) Conserved lipid-binding sites in membrane proteins: a focus on cytochrome c oxidase. *Curr. Opin. Struct. Biol. 17*, 444−450.

(20) Hanson, M., Cherezov, V., Roth, C., Griffith, M., Jaakola, V.-P., Chien, E., Valasquez, J., Kuhn, P., and Stevens, R. (2008) A specifc cholesterol binding site is established by the 2.8 Å structure of human β_2-adrenergic receptor in an alternate crystal form. *Structure 16*, 897−905.

(21) Adamian, L., Naveed, H., and Liang, J. (2011) Lipid-binding surfaces of membrane proteins:Evidence from evolutionary and structural analysis. *Biochem. Biophys. Acta 1808*, 1092−1102.

(22) Garcia, A., Sekowski, A., Subramanian, V., and Brasaemle, D. (2003) The central domain is required to target and anchor Perilipin A to lipid droplets. *J. Biol. Chem. 278*, 625−635.

(23) Miura, S., Gan, J. w., Brzostowski, J., Parisi, M. J., Schultz, C. J., Londos, C., Oliver, B., and Kimmel, A. R. (2002) Functional conservation for lipid storage droplet association among perilipin, ADRP, and TIP47 (PAT)-related proteins in mammals, Drosophila, and dictyostelium. *J. Biol. Chem. 277*, 32253−32257.

(24) Orlicky, D. J., DeGala, G., Greenwood, C., Bales, E. S., Russell, T. D., and McManaman, J. L. (2008) Multiple function encoded by the N-terminal PAT domain of adipophilin. *J. Cell Sci. 121*, 2921−2929.

(25) Hickenbottom, S. J., Kimmel, A. R., Londos, C., and Hurley, J. H. (2004) Structure of a lipid droplet protein: The PAT family member TIP47. *Structure 12*, 1199−1207.

(26) McManaman, J. L., Zabaronick, W., Schaack, J., and Orlicky, D. J. (2003) Lipid droplet targeting domains of adipophilin. *J. Lipid Res. 44*, 668−673.

(27) Chong, B. M., Russell, T. D., Schaack, J., Orlicky, D. J., Reigan, P., Ladinsky, M., and McManaman, J. L. (2011) The adipophilin C terminus is a self-folding membrane binding domain that is important for milk lipid secretion. *J. Biol. Chem. 286*, 23254−23265.

(28) Sander, C., and Schneider, R. (1991) Database of homology-derived protein structure and the structureal meaning of sequence alignment. *Protein: Struct., Funct. Genet. 9*, 56−68.

(29) Davidson, W., Jonas, A., Clayton, E., and George, J. (1998) Stabilization of α-synuclein secondary structure upon binding to synthetic membranes. *J. Biol. Chem. 273*, 9443−9449.

(30) Eliezer, D., Kutluay, E., Bussell, R., and Browne, G. (2001) Conformational properties of α-synuclein. *J. Mol. Biol. 307*, 1061−1073.

(31) Hynson, R., Jeffries, C., Trewhella, J., and Cocklin, S. (2012) Solution structure studies of monomeric human TIP47/perilipin-3 reveal a highly extended conformation. *Proteins 80*, 2046−2055.

(32) Bulankina, A., Deggerich, A., Wenzel, D., Mutenda, K., Wittmann, J., Rudolph, M., Burger, K., and Honing, S. (2009) TIP47 functions in the biogenesis of lipid droplets. *J. Cell Biol. 185*, 641−655.

(33) Atshaves, B. P., Petrescu, A. D., Starodub, O., Roths, J. B., Kier, A. B., and Schroeder, F. (1999) Expression and intracellular processing of the 58 KDa SCP-x/3-oxoacyl-CoA thiolase in transfected mouse L cells. *J. Lipid Res. 40*, 610−622.

(34) Hansson, M. D., Rzeznicka, K., Rosenback, M., Hansson, M., and Sirijovski, N. (2008) PCR-mediated deletion of plasmid DNA. *Anal. Biochem. 375*, 373−375.

(35) Hopp, T. P., and Woods, K. R. (1981) Prediction of protein antigenic determinants from amino acid sequences. *Proc. Natl. Acad. Sci. U. S. A. 78*, 3824.

(36) Rost, B., and Sander, C. (1994) Combing evolutionary information and neural networks to predict protein secondary structure. *Proteins 19*, 55−72.

(37) Jones, D. T. (1999) Protein secondary structure prediction basedo on position-specific scoring matrices. *J. Mol. Biol. 292*, 195−202.

(38) McGuffin, L. J., Bryson, K., and Jones, D. T. (2000) The PSIPRED protein structure prediction server. *Bioinformatics 16*, 404−405.

(39) Karplus, K., Karchin, R., Barrett, C., Tu, S., Cline, M., Diekhans, M., Grate, L., Casper, J., and Hughey, R. (2001) What is the value added by human intervention in protein structure prediction? *Proteins: Struct. Funct. Genet. Suppl. 5*, 86–91.

(40) Adamczak, R., Porollo, A., and Meller, J. (2005) Combining prediction of secondary structure and solvent accessibility in proteins. *Proteins: Struct. Funct. Genet. 59*, 467–475.

(41) Bernstein, F., Koetzle, T., Williams, G., Meyer, E., Brice, M., Rodgers, J., Kennard, O., Shimanouchi, T., and Tasumi, M. (1977) The protein data bank: A computer-based archival file for macro-molecular structures. *Eur. J. Biochem. 80*, 319–324.

(42) Marti-Renom, M. A., Stuart, A., Fiser, A., Sanchez, R., Melo, F., and Sali, A. (2000) Comparative protein structure modeling of genes and genomes. *Annu. Rev. Biophys. Biomol. Struct. 29*, 291–325.

(43) Eswar, N., Mari-Renom, M. A., Webb, B., Madhusudhan, M. S., Eramian, D., Shen, M., Pieper, U., and Sali, A. (2006) Comparative protein structure modeling with MODELLER. *Curr. Protocols Bioinformatics Suppl. 15*, 5.6.1–5.6.30.

(44) Landau, M., Mayrose, I., Rosenberg, Y., Glaser, F., Martz, E., Pupko, T., and Ben-Tal, N. (2005) Con/Surf 2005: The projection of evolutionary conservation scores of residues on protein structures. *Nucleic Acids Res. 33*, W299–W302.

(45) Glaser, F., Pupko, T., Paz, I., Bell, R. E., Bechor, D., Martz, E., and Ben-Tal, N. (2003) ConSurf: Identification of functional regions in proteins by surface-mapping of phylogenetic information. *Bioinformatics 19*, 163–164.

(46) Young, A., Scapin, G., Kromminga, A., Patel, S., Veerkamp, J., and Sacchettini, J. (1994) Structural studies on human muscle fatty acid binding at 1.4 A resolution: binding interactions with three C18 fatty acids. *Structure 2*, 523–534.

(47) Morth, J., Pedersen, P., Toustrup-Jensen, M., Sorensen, T., Petersen, J., Andersen, J., Vilsen, B., and Nissen, P. (2007) Crystal structure of the sodium-potassium pump. *Nature 450*, 1043–1049.

(48) Zavodszky, M. I., Sanschagrin, P. C., Korde, R. S., and Kuhn, L. A. (2002) Distilling the essential features of a protein surface for improving protein-ligand docking, scoring and virtual screening. *J. Comput.-Aided Mol. Des. 16*, 883–902.

(49) Thumser, A. E. A., and Wilton, D. C. (1994) Characterization of binding and structural properties of rat liver fatty-acid-binding protein using tryptophan mutants. *Biochem. J. 300*, 827–833.

(50) Rawel, H., Frey, S., Meidtner, K., Kroll, J., and Schweigert, F. (2006) Determining the binding affinities of phenolic compounds to proteins by quenching of the intrinsic tryptophan fluorescence. *Mol. Nutr. Food Res. 50*, 705–713.

(51) Hostetler, H., Kier, A., and Schroeder, F. (2006) Very-long-chain and branched-chain fatty acyl-CoAs are high affinity ligands for the peroxisome proliferatror-activated receptor α (PPARα). *Bio-chemistry 45*, 7669–7681.

(52) Senthivinayagam, S., McIntosh, A. L., Moon, K. C., and Atshaves, B. P. (2013) Plin2 inhibits cellular glucose uptake through interactions with SNAP23, a SNARE complex protein. *PLoS One 8*, e73696 DOI: 73610.71371/journal.pone.0073696.

(53) Lakowicz, J. (1999) *Principles of Fluorescence Spectroscopy*; Kluwer Academic/Plenum Publishers, New York.

(54) Sreerama, N., and Woody, R. W. (2000) Estimation of protein secondary structure from circular dichroism spectra: comparison of CONTIN, SELCON, and CDSSTR methods with an expanded reference set. *Anal. Biochem. 287*, 252–260.

(55) Teale, F., and Weber, G. (1957) Ultraviolet flurescence of the aromatic amino acids. *Biochem. J. 65*, 476–482.

(56) Frolov, A., and Schroeder, F. (1998) Acyl coenzyme A binding protein. Conformational sensitivity to long chain fatty acyl-CoA. *J. Biol. Chem. 273*, 11049–11055.

(57) Frolov, A., and Schroeder, F. (1998) Acyl Coenzyme A Binding Protein. *J. Biol. Chem. 273*, 11049–11055.

(58) Breiter, D. R., Kanost, M. R., Benning, M. M., Wesenberg, G., Law, J. H., Wells, M. A., Rayment, I., and Holden, H. M. (1991) Molecular structure of an apolipoprotein determined at 2.5-Å resolution. *Biochemistry 30*, 603.

(59) Ajees, A. A., Anantharamaiah, G. M., Mishra, V. K., Hussain, M. M., and Murthy, K. H. M. (2006) Crystal structure of human apolipoprotein A-I: Insights into its protective effect against cardiovascular diseases. *Proc. Natl. Acad. Sci. U. S. A. 103*, 2126.

(60) Dixon, T., Edwards, D., Cole, D., and Lapthorn, A. (2001) The structure of a zeta class glutathione S-transferase from Arabidopsis thaliana: characterisation of a GST with novel active-site architecture and a putative role in tyrosine catabolism. *J. Mol. Biol. 308*, 949–962.

(61) Choi, S., Tucker, D., Gross, D., Easton, R., DiPilato, L., Dean, A., Monks, B., and Brnbaum, M. (2010) Insulin regulates adipocyte lipolysis via an Akt-independent signaling pathway. *Mol. Cell. Biol. 30*, 5009–5020.

(62) Brasaemle, D., Bolios, G., Shapiro, L., and Wang, R. (2004) Proteomic analysis of proteins associated with lipid droplets of basal and lipolytically stimulated 3T3-L1 adipocytes. *J. Biol. Chem. 279*, 46835–46842.

(63) Brasaemle, D. L., Levin, D. M., Adler-Wailes, D. C., and Londos, C. (2000) The lipolytic stimulation of 3T3-L1 adipocytes promotes the translocation of hormone-sensitive lipase to the surfaces of lipid droplets. *Biochim. Biophys. Acta 1483*, 251–262.

(64) Tansey, J. T., Huml, A. M., Vogt, R., Davis, K. E., Jones, J. M., Fraser, K. A., Brasaemle, D. L., Kimmel, A. R., and Londos, C. (2003) Functional studies on native and mutated forms of perilipins. A role in protein kinase A-mediated lipolysis of triacylglycerols in Chinese hamster ovary cells. *J. Biol. Chem. 278*, 8401–8406.

(65) Buhrow, L., Ferguson-Miller, S., and Kuhn, L. (2012) From static structure to living protein:Computational prediction and validation of cytochrome c oxidase flexibility. *Biophys. J. 102*, 2158–2166.

(66) Melikyan, G., Markosyan, R., Hemmati, H., Delmedico, M., Lambert, D., and Cohen, F. (2000) Evidence that the transition of HIV-1 Gp41 into a six-helix bundle, not the bundle configuration, induces membrane fusion. *J. Cell Biol. 151*, 413–424.

(67) Welker, S., Rudolph, B., Frenzel, E., Hagn, F., Liebisch, G., Schmitz, G., Scheuring, J., Kerth, A., Blume, A., Weinkauf, S., Haslbeck, M., Kessler, H., and Buchner, J. (2010) Hsp12 is an intrinsically unstructured stress protein that folds upon membrane association and modulates membrane function. *Mol. Cell 39*, 507–520.

(68) Patel, S., Yang, W., Kozusko, K., Saudek, V., and Savage, D. (2014) Perilipins 2 and 3 lack a carboxy-terminal domain present in perilipin1 involved in sequestering ABHD5 and supressing basal lipolysis. *Proc. Natl. Acad. Sci. U. S. A. 111*, 9163–9168.

(69) Wang, H., Sreenevasan, U., Hu, H., Saladino, A., Polster, B. M., Lund, L. M., Gong, D. W., Stanley, W. A., and Sztalryd, C. (2011) Perilipin 5, a lipid droplet-associated protein, provides physical and metabolic linkage to mitochondria. *J. Lipid Res. 52*, 2159–2168.